The FUll Retrieval Method [FURM] Analysis of the Effects of Biomass Burning Emissions on Tropical Tropospheric Ozone

By

Amao Olayinka Akeem

A thesis submitted to the Institute of Environmental Physics and Remote Sensing, University of Bremen in partial fulfilment of the requirements for the award of the degree of Masters of Science in Environmental Physics.

September, 2003

Declaration

I herewith declare that I did the written work on my own and only with the means as indicated.

date and signature

_____

Tutor:

Dr. A. Ladstätter-Weißenmayer

_____

Supervisor:

Prof. Dr. J. P. Burrows

Contents

List of Figures Page

List of Tables Page

ABSTRACT

In 1997, wildfire burned extensively in Indonesia, South America and Africa. Attention was mostly drawn to Indonesia because of the severity of the fire mainly due to the 1997 EL-Niño event. This leads to emission of NO_x (NO + NO_2) and VOCs and subsequently leading to photochemical production of tropospheric ozone.

In order to investigate the effects of these emissions on tropospheric ozone production, the FUll Retrieval Method (FURM) Algorithm was used to derive the tropospheric ozone vertical column for Watukosek, Indonesia not only for the year 1997, but also for 1998.

The FUll Retrieval Method [Rozanov] was developed at the Institute of Remote sensing, University of Bremen to enable the retrieval of height resolved ozone information from GOME sun normalized spectra. It uses temperature dependence absorption in the Hartley-Huggins bands of ozone. It is made up of two major parts:-

A forward Model, based on the radiative transfer model (RTM) GOMETRAN *[Rozanov,1997]* which calculates the top of the atmosphere (TOA) radiance and the weighting functions for a given state of the atmosphere as defined by, the Ozone vertical distribution; trace gas distribution; surface albedo, and aerosol scenario.

An Inversion Scheme which matches in iterative steps the calculated TOA radiance and the measured GOME radiance by modifying model atmospheric parameters such as the vertical distribution of ozone using an appropriate weighting function as defined by GOMETRAN.

So as to determine the retrieval efficiency of the FURM algorithm, the vertical column of tropospheric ozone was also derived for Hohenpeissenberg, Germany an area of urban pollution.

Finally, in a view validate the FURM algorithm the derived tropospheric ozone vertical column for Watukosek was compared to SHADOZ (Southern Hemisphere Additional OZonesondes) sonde measurements, while Hohenpeissenberg was compared to the DWD (Deutscher Wetterdienst) sonde measurements.

1 Introduction

1.1 Atmospheric Composition

The atmosphere is a relatively stable mixture of several gases during the day, the proportion of which, excluding water vapour, are nearly uniform up to approximately 80 km above the Earth's surface. The major components of this region, by volume, are oxygen (21%), nitrogen (78%), and argon (0.93%).

The atmosphere is thought of as a dynamic system, with its gaseous constituents continuously being exchanged with vegetation, oceans and biological organisms. The cycle of atmospheric gases involve a number of physical and chemical processes. Gases are produced chemically by biological activity, volcanic eruption, radioactive decay and human activities, while removal is through chemical reactions, physical processes, and deposition.

Also present are a number of trace gases that occur relatively in small and sometimes highly variable amounts. Even with this remarkably small composition, temperature and atmospheric chemistry are believed to be controlled by the trace gases. There is evidence that environmentally significant trace gases are changing because of both natural and human factors. Carbon dioxide (CO_2), nitrous oxide (N_2O), and methane (CH_4) are changing in concentration through actions like the burning of fossil fuels, biomass burning, expulsion from living and dead biomass, release from metabolic processes of micro-organisms in the soil, industries and traffic, and oceans of our planet.

species	relative abundance (parts per billion by volume)	source	comment
N_2	7.81×10^8	biologic	long lived
O_2	2.01×10^8	biologic	long lived
H_2O	$10^6 - 10^7$	physical	long lived
Ar	9.34×10^6	radiogenic	permanent
CO_2	3.5×10^5	biologic, industrial	variable, increasing
Ne	1.8×10^4	interior	permanent
He	5.2×10^3	radiogenic	escaping
CH_4	1.6×10^3	biologic	variable, increasing
Kr	1.0×10^3	interior	permanent
H_2	5.0×10^2	biologic, photochemical	variable
N_2O	3.0×10^2	biologic, industrial	increasing
CO	1.0×10^2	photochemical, industrial	variable, increasing
SO_2	$<10^2$	industrial, photochemical	variable
O_3	$<10^2$	photochemical	variable
Xe	9×10^1	interior	permanent
NO, NO_2, NO_x	variable	industrial, biologic	—*
CH_3Cl	6.0×10^{-1}	biologic	short lived
CCl_2F_2	2.9×10^{-1}	industrial	increasing
CCl_3F	1.7×10^{-1}	industrial	increasing
CCl_4	1.2×10^{-1}	industrial	increasing
CH_3CCl_3	9.8×10^{-2}	industrial	increasing
CF_4	7.0×10^{-2}	industrial	increasing
CH_3Br	1.0×10^{-2}	biologic, industrial	possibly increasing

*Relatively short lived, with an average lifetime of roughly one month.

Table 1.1 List of some major and atmospheric trace gases [http://www.c-f-c.com/charts/atmosph.htm]

1.2 Major Atmospheric Layers

The gaseous area surrounding the planet is divided into several concentric spherical layers or strata, separated by narrow transition zones (see figure 1.1), and are characterized by differences in chemical composition.

1.2.1 Troposphere

The troposphere (region of mixing) because of the vigorous convective air current prevalent within the layer is the atmospheric layer closest to the planet and contains the largest percentage of the mass of the total atmosphere. The surface layer of the troposphere is known as the planetary boundary layer, which extends vertically to between a few hundred meters and about 2 km. This layer interacts directly with the earth surface, and so it is important for the transfer of surface emissions into the troposphere. Emitted species become very well mixed in the boundary layer and are then mixed out into the free troposphere.

Chemical processes play a central role in determining the behaviour and composition of earth's troposphere. The chemical transformations that occur in the atmosphere contribute to the changes in the distributions of trace gases (e.g. ozone), and so affect other atmospheric systems.

Approximately 10% of total atmospheric ozone resides here, where it serves as a greenhouse gas in the upper troposphere. However in the lower troposphere, ozone is a pollutant, which is harmful to plants and animals because of its toxicity.

The upper boundary layer ranges in height from 8 km in high latitudes, to 17 km above the equator. Its height varies with the seasons: highest in the summer and lowest in the winter. Temperature decreases with increasing altitude, however

within the tropopause (which) separates the troposphere from the stratosphere, temperature remains constant.

1.2.2 Stratosphere

The stratosphere is the second major stratum of air in the atmosphere. It resides between 10 and 50 km above the planet's surface. The air temperature in the stratosphere increases gradually with altitude to 200-220 degrees Kelvin (K) at the lower boundary of the stratopause (~50 km), which is marked by a decrease in temperature. Because the air temperature in the stratosphere increases with altitude, it does not cause convection and has a stabilizing effect on atmospheric conditions in the region.

Ozone plays the major role in regulating the thermal regime of the stratosphere. Solar energy is converted to kinetic energy when ozone molecules absorb ultraviolet radiation in the wavelength range from 290 nm to 320 nm resulting in heating of the stratosphere. The ozone layer is located at an altitude of approximately 10-35 km. Approximately 90 % of the ozone in the atmosphere resides in the stratosphere. Table 1.2 gives a brief summary of the differences between the troposphere and the stratosphere.

Stratosphere	Troposphere
Low Pressure	High Pressure
High UV radiation	Low UV Radiation
Low Temperature	High Temperature
Few Sinks	Many Sinks
Few Sources	Many Sources
Less anthropogenic Impact	Much anthropogenic Impact
Low Vertical Mixing	Strong Vertical Mixing
Low Humidity	High Humidity

Table 1.2 Important differences between the stratosphere and the troposphere

Meteorological conditions strongly affect the distribution of ozone. Most ozone production and destruction occurs in the tropical upper stratosphere, where the largest amounts of ultraviolet radiation are present.

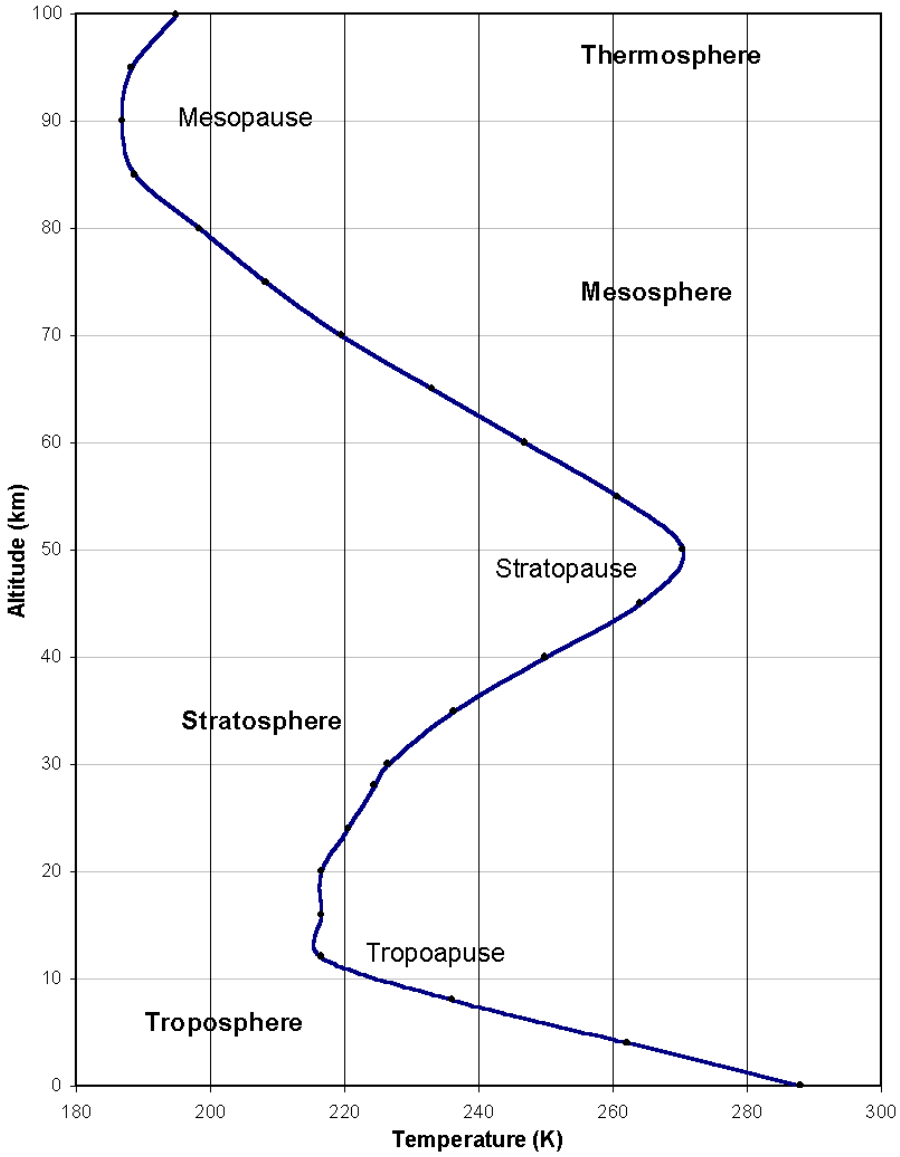

Figure 1.1 Atmospheric Structure showing the temperature profile. To the four regions correspond very different temperature gradients.

1.3 The Earth's Heat Balance and the Greenhouse Effect

The global energy balance is the balance between incoming energy from the sun and outgoing heat from the earth. It regulates the state of the earth's climate, and modifications to it as a result of natural and man-made climate forcing, cause the global climate to change energy released from the sun as electromagnetic radiation. The sun has a temperature of approximately 6000°K. At this temperature, electromagnetic radiation is emitted as short-wave light and ultraviolet energy, and travels across space at the speed of light. When it reaches the earth's surface, some is reflected back to space by clouds, air molecules and the earth surface – albedo of the earth. The atmosphere absorbs some, and some is absorbed at the earth's surface.

The earth releases a lot of energy it has received from the sun back to space. However, since the earth is much cooler than the sun, its radiating energy is longer wavelength infrared energy or heat. The energy received by the earth from the sun balances the energy lost by the earth back into space. In this way, the earth maintains a stable average temperature and therefore a stable climate (although of course differences in climate exist at different locations around the world).

The earth atmosphere contains a number of greenhouse gases such as CO_2, CH_4, N_2O, and O_3 which absorb electromagnetic radiation at some wavelengths but allow radiation at other wavelengths to pass through unimpeded. It is mostly transparent in the visible light (which is why we can see the sun), but significant

blocking (through absorption) of ultraviolet radiation by the ozone layer, and infrared radiation by greenhouse gases, occurs.

The absorption of infrared radiation trying to escape from the earth back to space is particularly important. Such energy absorption by the greenhouse gases heats the atmosphere, and so the earth stores more energy near its surface than it would if there was no atmosphere. The average surface temperature of the moon for instance (about the same distance as the Earth from the Sun) is 255K. The moon, of course, has no atmosphere. By contrast, the average surface temperature of the earth is 288K. This heating effect is called the **natural greenhouse effect.**

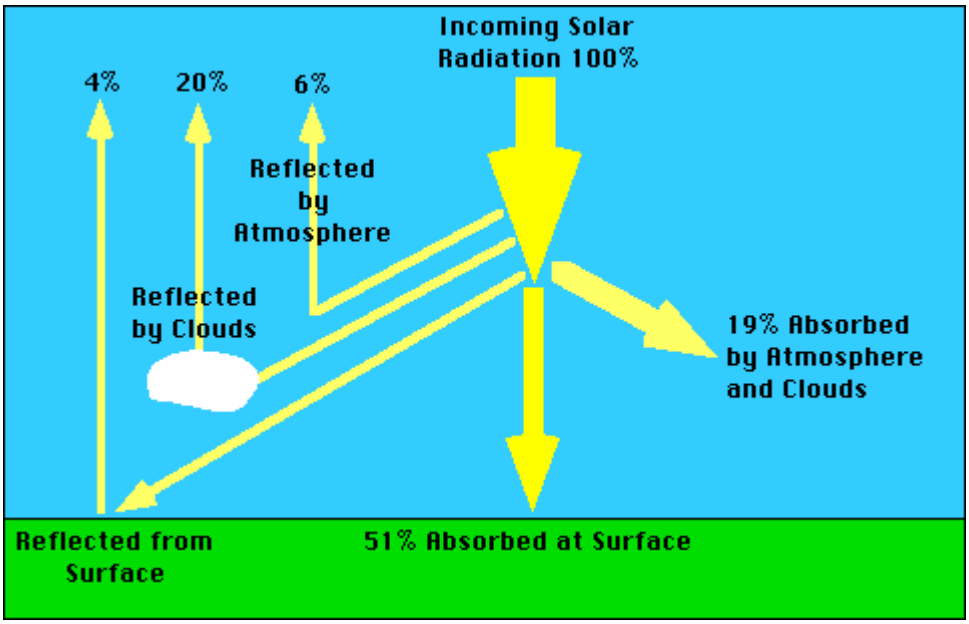

Figure 1.2 the greenhouse effect, showing absorption and the reflection of solar and longwave radiation

1.4 Atmospheric Ozone

During the last two decades, the word “ozone” and the phrase “ozone layer” have come into everyday usage, and even the descriptions of “good” ozone and “bad” ozone are commonly heard. More remarkably, the adjectives convey correctly the qualitative significance of the effects of ozone in different parts of the atmosphere. Ozone, the triatomic form (O_3) of oxygen, accounts for only 3 molecules of every 10 million in Earth's atmosphere where it is spread very unequally (see section 1.2). The peak concentration is recorded at between the 10 and 35 km altitude (see figure 1.3) – the so-called ozone layer. Sequential decline however occurs in this layer leading to the ozone hole phenomenon [Farman, 1985].

Stratospheric ozone is formed by the action of solar ultraviolet (UV) radiation on ordinary molecular oxygen (O_2). It is a strong absorber of UV radiation, especially the most harmful, and reacts readily with many other molecules.

In lower atmosphere, there has been reported increase in its concentration from biomass and fossil fuel burning and so having a negative impact on the health of living organisms. The difference between the good and the bad ozone lies in its ability to react, usually deleteriously, with the molecules, which make up the surfaces of biological species, e.g. the lining of human lungs, or the leaves of green plants.

The scientific aim of this study is to investigate the impact of biomass burning emissions and urban pollution on the oxidation power of the troposphere [Ladstätter Weißenmayer et al.,1999] with focus on ozone production by analysing ozone-sonde data and satellite based GOME data using the FUll Retrieval Method algorithm [Rozanov, 1997].

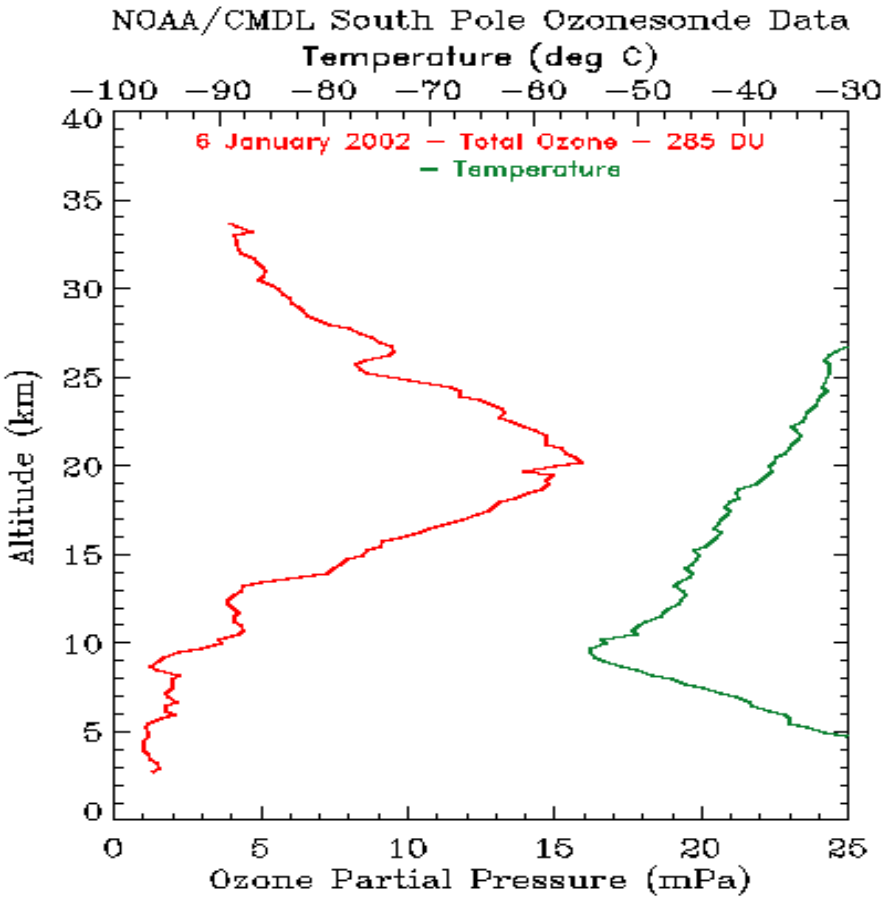

Figure 1.3 Distribution of ozone in the atmosphere [NOAA/CMDL South Pole Ozonesonde Data]. The red curve shows the ozone profile from ground level to about 35 km altitude; the green curve is the temperature profile.

2 Tropospheric Chemistry

2 .1 Tropospheric Ozone

Despite it's rather small percentage of in this layer, ozone plays a major role in determining the chemistry of the troposphere.

2.1.1 Roles of Ozone in the Troposphere

In the upper troposphere, ozone serves as a greenhouse gas, thereby contributing to the greenhouse effect (see section 1.3).

It is also the major source of the tropospheric hydroxyl radicals (OH).

Ozone is photolysed by sunlight (λ < 340nm) to an excited oxygen atom O (^1D) and an oxygen molecule (O_2), where a further reaction of the O (^1D) with H_2O molecule leads to the formation of two molecules of OH radicals (see R1 and R2 below).

$$O_3 + hv \rightarrow O(^1D) + O_2 \qquad \text{R1}$$

$$O(^1D) + H_2O \rightarrow 2OH \qquad \text{R2}$$

However, only about 1% of the O (^1D) from R1 reacts with the H_2O, as most collisionally transfer their excitation by quenching and return to the ground state oxygen atom O(^3P), which then reacts with O_2 to reproduce O_3 [Levy et al., 1971] (see R3 and R4)

$$O(^1D) + M \rightarrow O(^3P) + M \qquad \text{R3}$$

$$O(^3P) + O_2 + M \rightarrow O_3 + M \qquad \text{R4}$$

where M (O_2 or N_2) is a collision partner.

OH radical is the most important tropospheric oxidizing agent. It initiates most oxidation processes of many volatile organic compounds (VOCs) such as, carbon monoxide (CO), hydrocarbons (HCs) and non-methane hydrocarbons (NMHCs). This makes the concentration of tropospheric O_3 important in determining the oxidizing capacity of this lower atmosphere.

Despite these rather positive aspects, ground level O_3 is highly toxic and in the presence of nitrogen oxides (NO_x = NO + NO_2) and VOCs leads to photochemical smog situations.

There has been evidence that the concentration of tropospheric ozone has increased by about 1% per annum in the last 20 years [WMO, 1991] as a result of population increase and subsequently increases in emissions of NO_x and VOCs from urban and biomass burning related pollution.

2.1.2 Sources of Tropospheric Ozone

There are two sources for tropospheric ozone;

1) Stratospheric-Tropospheric Exchange (STE). Ozone is formed in the stratosphere from O_2 photolysis by short-wave ultraviolet radiation ($\lambda < 240$ nm) mostly in the tropics. This is then transported into the troposphere by the so-called Brewer-Dobson circulation.

2) The main anthropogenic source of ozone in the troposphere however is through the photolysis of NO_2 ($\lambda < 420$ nm) to nitric oxide (NO) and atomic oxygen (O). A further reaction of the O atom with O_2 yields ozone (see R5 and R6 below).

$$\mathbf{NO_2 + hv \rightarrow NO + O} \qquad \mathbf{R5}$$

$$\mathbf{O + O_2 + M \rightarrow O_3 + M} \qquad \mathbf{R6}$$

M = collision partner (O_2 or N_2)

O_3 itself being highly chemically reactive reacts with NO to return NO_2.

$$O_3 + NO \rightarrow NO_2 + O_2 \qquad R7$$

If j_5 is the photolysis rate for R5, and K_6 and k_7 are reaction rate coefficients for reactions R6 and R7 respectively, then the rate equation for NO_2 can be written as

$$d[NO_2]/dt = k_7 [NO][O_3] - j_5 [NO_2] \qquad 2.1$$

If this equation is considered steady-state, then it can be set to zero and the equilibrium concentration of ozone can be determined from: -

$$[O_3] = J_5 [NO_2]/ k_7 [NO] \qquad 2.2$$

this is the photo-stationary state relationship.

However, the mixing ratio of O_3 measured in urban and regional troposphere are often greater than those calculated from the photo-stationary state relationship. This implies that other reactions than (R5) – (R7) are important.

Elevated level of O_3 is achieved in the troposphere as a result of reactions involving NO_x, CO, HCs and NMHCs in the presence of hydrogen oxides and sunlight.

Increase in the emissions of these O_3 precursors over the past century from fossil fuel and biomass burning are believed to have resulted in increase in the tropospheric O_3 concentrations over industrial regions and probably on a global scale.

2.2 Urban Air Pollution and Photochemical Smog

An *air pollutant* is "any gas or particulate that, at high enough concentrations, may be harmful to life and/or property" [Matthias 1996]. There are both natural and anthropogenic sources of air pollution. Natural sources include volcanic eruptions, dust storms, oceans, vegetation, and accidental forest fires caused by lightning. Anthropogenic sources are numerous and generally emit far greater quantities of air pollutants than any natural source [Boubel et al. 1994; Wysocki 1998; Matthias 1996].

Urban pollution occurs in big cities from the burning of fossil fuels, transportation and industries. It can be in the form of secondary pollutants such as photochemical smog, acid rain (HNO_3, H_2SO_4) or, primary pollutants like CO, particulate matter, NO_x and VOCs.

Smog is chemical mixture of gases that forms a brownish-yellow haze primarily over urban areas. Components of smog include ground-level O_3, NO_x, VOCs and particulate matter. These gases result from a reaction between certain airborne pollutants and strong sunlight. Smog is most prevalent in the summer months, when there is the most sunlight and temperatures are the highest. In large enough quantities, it poses threats to animal, plant, and human life. The airborne pollutant, which makes up 90% of all smog found in urban areas, is ground level O_3.

The formation of ground level O_3 occurs as a result of chemical reactions between several distinct forms of pollutants and sunlight.

Two groups of chemical pollutants are involved in photochemical smo: NO_x, and VOCs.

When stagnant air masses linger over urban areas, the pollutants are held in place for long time period. Sunlight interacts with these pollutants, transforming them into O_3, which remains in the lower atmosphere until weather systems flush out a given area and dissipate them. An episode of ground level O_3 can last from several hours to several days and are particularly severe in cities with high concentrations of NO_x and VOCs during periods of warm weather.

Figure 2.1 illustrates the daily variation in the key chemical players. The diagram suggests:

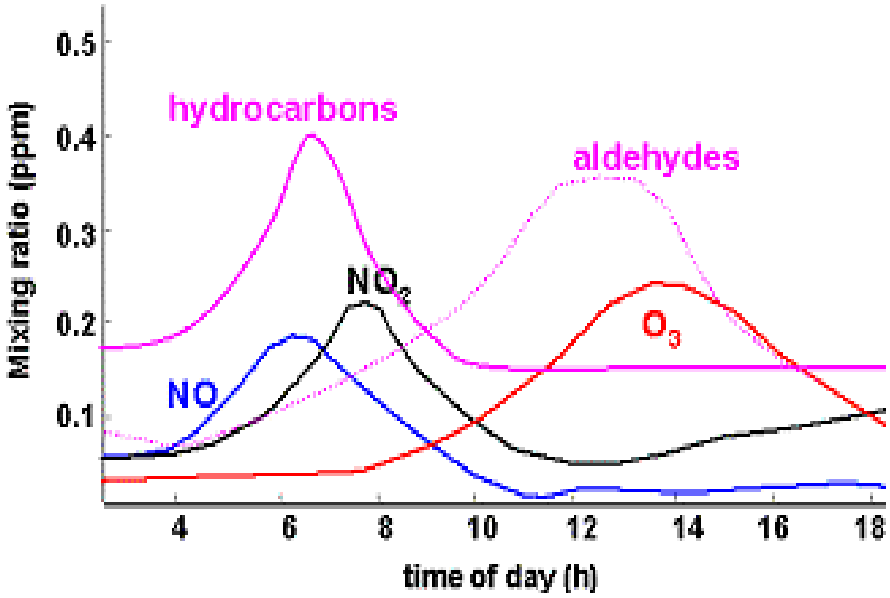

Figure 2.1 Evolution of the concentration of NO_x, O_3, hydrocarbon and aldehydes

Early morning traffic increases the emissions of both NO_x and VOCs as people drive to work. Later in the morning, traffic dies down and the NO_x and VOCs begin to react forming NO_2, increasing its concentration.

As the sunlight becomes more intense later in the day, NO_2 is broken down and its by-products form, increasing concentrations of O_3. At the same time, some of the NO_2 can react with the VOCs to produce toxic chemicals such as Peroxyacetyl Nitrate (PAN).

As the sun goes down, the production of O_3 is halted and the remaining is then consumed by several different reactions. Despite the degradation of O_3 during the night, the level increases from day to day during a smog episode.

Several meteorological factors such as precipitation, wind, temperature inversion, and topography can also influence the formation of photochemical smog.

Figure 2.2 New York City under a typical smog situation.

2.3 Biomass Burning

Crutzen in 1979 first made the first suggestion that global vegetation fires might contribute significantly to the concentration of atmospheric trace gases. Since then, evidence from several field experiments such as SCAR (Smoke Cloud And radiation) and BIBEX (Biomass Burning Experiment) have shown that biomass burning in its various forms represent a major perturbation of atmospheric chemistry.

Literarily meaning the combustion of living and recently dead plants material, both for sustainable (active fire management of ecosystem) and non-sustainable (clearing and conversion of areas of natural vegetation) objectives.

The main biomass burning seasons are, December till February when fires in the Northern Africa occur, September-March when vegetation fires occur in Southern Africa, Southern America and Southern Asia, while most extra-tropical fires occur from June till August in the boreal regions, i.e., Canada and Russia (see figure 2.3)

The immediate effect of burning is the production and release into the atmosphere of gases and particulates that result from the combustion of biomass matter. The instantaneous combustion products of burning vegetation include carbon dioxide, carbon monoxide, methane, non-methane hydrocarbon, nitrogen oxides, oxygenated hydrocarbon (e.g HCHO), methyl bromide (CH_3Br), methyl chloride (CH_3Cl) and various particulates.

Biomass burning clearly has the potential to greatly modify tropospheric chemistry as the main emitted gases play divergent roles in impacting the global climate and environment.

Photochemical production of tropospheric ozone is highly enhanced via the oxidation of CO, CH_4, and NMHCs by the hydroxyl radical in presence of nitrogen oxides (see section 2.4). The chemical lifetime of some of the oxygenated hydrocarbon is rather short, leading to a rapid ozone production during the first hours after the emission.

On a regional scale, biomass burning emissions increase the concentration of the longer-lived organic compounds (see table 2.1) and therefore increase photochemical ozone production also on a regional scale. From global simulations, it was inferred that biomass burning is responsible for approximately 10% of the global annual tropospheric ozone concentration. However, on a local and regional scale, the impact could be much higher.

Aside it's role in tropospheric ozone production, emissions from biomass burning are also a major source of cloud condensation nuclei (CCN), which could affect microphysics of clouds, thus altering the earth's radiative budget through the modification of the cloud albedo. NO_2 also reacts with OH to produce nitric acid (HNO_3, see R8) - a component of acid precipitation.

$$\mathbf{NO_2 + OH + M \rightarrow HNO_3 + M} \qquad \mathbf{R8}$$

Biomass burning accounts for approximately 39% of total tropical tropospheric ozone production and about 25% of the global greenhouse gases (CO_2 and CH_4) emission and so contribute to the greenhouse effect [Kaufman et al., 1992].

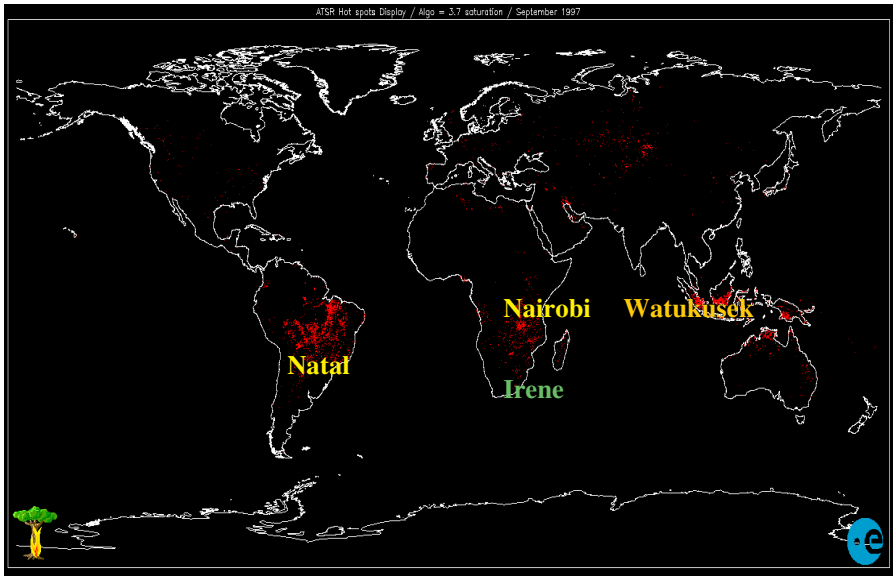

Figure 2.3 Biomass burning occurs almost every year in the tropical regions of Africa, Latin America and Southeast Asia during the dry season. The red spots indicate major Biomass Burning areas [ATSR World Fire Atlas, September1999].

Generally, over regional to global scales the amount of biomass burned per year is estimated to be [Seiler and Cruitzen, 1980]:

$$M = A * B * \alpha * \beta \qquad 2.3$$

where,

M = Estimated amount of dry biomass burned

A = Burned area

B = Biomass density

α = Aboveground biomass

β = Fraction of aboveground biomass burned.

From this approach, the amount of biomass burned for all the tropics per year is estimated at $5 * 10^9$ tons/year [Hao et al., 1990].

2.4 Photochemical Ozone Production from NO_x and VOCs

There are hundreds of different organic compounds involved in the photochemical production of tropospheric ozone. Their involvement in the photochemistry depends on their ability to form free radicals by chemical reactions through sunlight-driven photolysis.

The OH radical initiates most of this oxidation processes (see sections 2.4.1 – 2.4.3).

Once an organic compound reacts with a free radical, the successive oxidation steps, which lead to the formation of ozone, may be quite rapid provided the nitrogen oxides (NO_x, mainly as NO) concentration is at least 10-40 ppt. Some of the intermediate species may reach detectable concentrations during photochemical episodes. Such intermediates include organic nitrogen compounds such as peroxyacetyl nitrate, aldehydes (e.g. formaldehyde), carbon monoxide and hydrogen peroxide (H_2O_2).

2.4.1 CO Oxidation – O_3 Production

Carbon monoxide is produced as a by-product of incomplete combustion of carbon-containing materials as well as due to photochemical conversion of atmospheric methane and other hydrocarbons. The main sources of CO are located at continental surfaces; the most important of them are human-related emissions (year-round) and biomass burning (dry seasons in tropics and warm part of the year in boreal areas). Photochemical conversion of hydrocarbons, e.g., methane, is an important source of CO, especially in summertime and the tropics. CO is usually the dominant sink for OH, although other species in polluted or forested areas can be important [Brune, this issue, 1997; Wang, this issue, 1997].

As a result, OH distributions and trends could influence CO concentration dramatically.

CO reacts with the OH radical in a chain reaction to yield NO_2 as shown below.

$CO + OH \rightarrow CO_2 + H$	R9
$H + O_2 + M \rightarrow HO_2 + M$	R10
$HO_2 + NO \rightarrow NO_2 + OH$	R11
$NO_2 + h\nu \rightarrow NO + O$	(R5)
$O + O_2 + M \rightarrow O_3 + M$	(R6)
$Net: CO + 2O_2 + h\nu \rightarrow CO_2 + O_3$	R12

2.4.2 Hydrocarbon Oxidation Cycle – O_3 Production

The most common reaction of the hydroxyl radical is called "hydrogen abstraction." In hydrogen abstraction reactions a hydrogen atom from another substance is added to the hydroxyl radical, converting the hydroxyl radical to a water molecule and simultaneously generating a new radical on the substance, which lost the hydrogen atom. The steps in the reaction of hydroxyl radical with the simplest hydrocarbon (methane) are shown below: -

$CH_4 + OH \rightarrow CH_3 + H_2O$	R13
$CH_3 + O_2 + M \rightarrow CH_3O_2 + M$	R14
$CH_3O_2 + NO \rightarrow NO_2 + CH_3O$	R15
$CH_3O + O_2 \rightarrow CH_2O + HO_2$	R16

$$HO_2 + NO \rightarrow NO_2 + OH \qquad R17$$

$$2(NO_2 + h\nu \rightarrow NO + O) \qquad R18$$

$$2(O + O_2 + M \rightarrow O_3 + M) \qquad R19$$

$$\textit{Net : } CH_4 + 2h\nu + 4O_2 \rightarrow CH_2O + H_2O + 2O_3 \qquad R21$$

HO_x, NO_x and tropospheric conditions catalyse this net reaction. The reactions of CH_3 and CH_3O with O_2 are so fast that they are usually assumed to be intermediates.

The gas phase oxidation of formaldehyde to CO occurs through photolysis at wavelengths below 370 nm in two channels (R22 and R23) or reaction with OH (R24) leading to production of HO_x radicals.

$$CH_2O + h\nu \rightarrow CO + H_2 \qquad R22$$

$$CH_2O + O_2 + h\nu \rightarrow CHO + HO_2 \qquad R23$$

$$CH_2O + OH \rightarrow H_2O + CHO \qquad R24$$

In a low NO_x environment reaction of the methylperoxy radical (CH_3O_2) with HO_2 may compete with reaction R15 ;

$$CH_3O_2 + HO_2 \rightarrow CH_3OOH + O_2 \qquad R25$$

forming the hydroperoxide (CH_3O_2H) which again can photolyze or react with OH,

$$CH_3O_2H + OH \rightarrow CH_3O_2 + H_2O \qquad R26$$

$$CH_3O_2H + h\nu \rightarrow CH_3O + OH \qquad R27$$

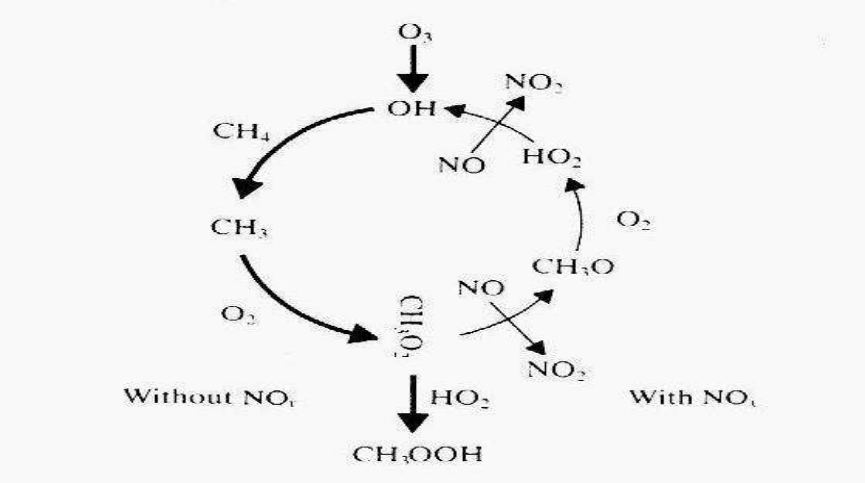

Figure 2.4 Schematic of the CH_4 oxidation cycle [Wayne, 1991]. The bold arrows in the first half of the cycle indicate what happens without NO_x, while the thin arrows on the second half indicate processes that require NO_x, and close the loop back to the formation of hydroxyl.

There is a general consensus that the average concentration of methane in the atmosphere is increasing at a current rate of nearly 1% per year in both hemispheres [WMO, 1991]. It is essentially due to the dramatic increase in agricultural and industrial emissions coupled to global population growth.

NO_x therefore plays a very important role in the methane oxidation cycle. If it is sufficiently abundant, it closes the loop of a cycle that regenerates hydroxyl. In its absence, the cycle terminates abruptly and methane becomes a sink for hydroxyl (see figure 2.4).

2.4.3 NHMCs Oxidation – O_3 Production

A large variety of non-methane hydrocarbons are formed throughout the troposphere and these can include alkanes (except methane), alkenes, aromatics, and biogenically produced compounds such as isoprenes and terpenes. The oxidation of NMHCs produce a variety of oxygenated products like, aldehydes, ketones, di-carbonyls, alcohols, phenols, peroxides, organic acids and organic nitrates.

Their reaction with the OH radical follows the same pattern as that of methane, but a much larger number of intermediate species are formed. An increase in their concentration in the troposphere will therefore have great consequences on the oxidation power of the troposphere.

They also produce odd-hydrogen species and organic radicals, so that they contribute to an increase in the concentration of peroxy (HO_2) radicals and odd-hydrogen radicals as a whole.

When HO_2 and RO_2 (R = hydrocarbon fraction) concentration are increased in the presence of sufficient NO, the formation of NO_2 is enhanced and thus an enhanced ozone production could be attained.

$$RH + OH \rightarrow R + H_2O \qquad R28$$

$$R + O_2 + M \rightarrow RO_2 + M \qquad R29$$

$$RO_2 + NO \rightarrow RO + NO_2 \qquad R30$$

$$RO + O_2 \rightarrow HO_2 + R'CHO \qquad R31$$

$$HO_2 + NO \rightarrow OH + NO_2 \qquad (R17)$$

$$2(NO_2 + hv \rightarrow NO + O) \qquad (R18)$$

$$2(O + O_2 + M \rightarrow O_3 + M) \qquad (R19)$$

$$\textit{Net : } RH + 4O_2 + 2hv \rightarrow R'CHO + H_2O + 2O_3 \qquad R32$$

Acetyl radicals (RCO_3) are also produced as intermediates where they form peroxyacetyl nitrate. PAN, organic nitrates and peroxy nitrites may carry reactive nitrogen to remote regions, thereby becoming a significant source of ozone precursors in remote locations.

The reactivity of individual hydrocarbons with respect to OH can vary greatly depending upon their molecular structure. This means that non-methane hydrocarbons released into the atmosphere can have lifetimes ranging from minutes to days. Table 2.1 shows a range of hydrocarbon compounds and their lifetimes in the atmosphere. The lifetimes are calculated assuming a diurnally averaged OH concentration of $2x10^6$ molecules cm^{-3} at temperature of 298°K.

In general CO, CH_4 and NMHCs oxidation coupled with the emission of NO_x leads to high tropospheric production of ozone.

In remote locations with low NO_x emissions the simplified equation for the OH radical can be written as: -

$$[OH] = 2k_2 [H_2O][O^1D]/(k_9 [CO]+k_{13}[CH_4]+ k_{28}[RH]) \quad 2.4$$

.

Species	k_{OH} / molec^{-1} s^{-1} x 10^{12} at 298K	Chemical Lifetime (w.r.t OH)
Ethane	0.268	22 days
Propane	1.15	5.0 days
i-Butane	2.34	2.5 days
n-Butane	2.54	2.3 days
i-Pentane	3.90	1.5 days
2-metylpentane	5.6	1.0 days
3-methylpentane	5.7	1.0 days
2,2-dimethylbutane	2.32	2.5 days
2,3-dimethylbutane	6.2	0.93days
Ethene	8.52	16 hours
Propene	26.3	5.3 hours
1-Butene	31.4	4.4 hours
Isoprene	101	1.4 hours

Table 2.1 OH reaction rate coefficients for a number of hydrocarbon compounds. Chemical lifetimes assume a diurnally average OH concentration of 2x10^{6} molecules cm^{-3}. [Goldan et al. 2000]

2.5 NO_x and VOCs Limited Regimes

A NO_x limited region is that region where the concentration of ozone depends on the amount of NO_x present in the atmosphere. This occurs when there is a lack of NO_2, thus inhibiting ozone titration when oxygen mixes with VOCs. In these regions, controlling the NO_x emission would reduce ozone concentrations.

A VOCs limited region is one where the concentration of ozone depends on the amount of VOCs in the atmosphere. Controlling VOCs here would reduce ozone concentrations.

Figure 2.4 gives a brief summary of the concept of the NO_x and VOCs limited regions for a better understanding.

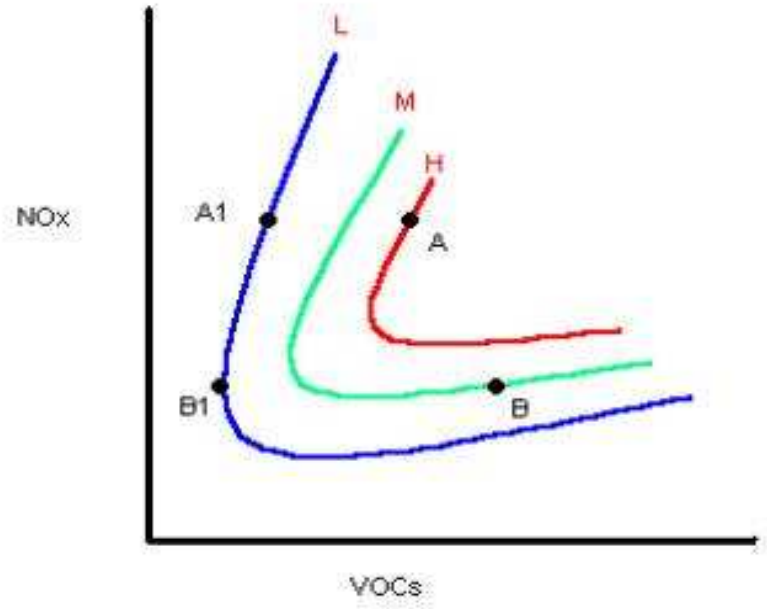

Figure 2.5 The Ozone Isopleth illustrating the concept of NO_x and VOCs limited

The above figure is broken down into three parts: -

The x-axis displays increasing concentrations of VOCs from left to right. The y-axis displays increasing concentrations of NO_x from bottom to top. The isopleths – the c-shaped curves (blue, green and red) represent increasing concentrations of ozone from the bottom left corner to the top right corner; ozone concentration remains constant along each isopleth, but changes between each isopleth.

The isopleths are used for determining ozone levels at specific combinations of NO_x and VOCs in the atmosphere and to determine whether a region is NO_x or VOCs limited. If a region is situated in the bottom right corner of the graph, it is NO_x limited since the amount of NO_x determines the amount of ozone created. This is because an increase in NO_x moves the point to another isopleth where an increase in VOCs only moves the point in question along the same isopleth, not increasing the ozone concentration.

At point A, the atmosphere is VOCs limited because changing the concentration of NO_x does not alter the ozone concentration, but changing the concentration of VOCs will alter the ozone concentration.

A change in NO_x at point B changes the ozone concentration, while changes in VOCs does not. This point is therefore a NO_x limited region.

2.6 Ozone in the Tropical Troposphere

The oxidizing capacity of the troposphere - the ability of the troposphere to remove pollutants emitted, depends on strongly on the abundance of ozone in the tropics. The tropic is that region of the earth that lies between approximately 23.5°N and 23.5°S of the equator (see figure 2.6). As large amounts of biomass burning take place during the dry season in the tropical regions, also large amounts of NO_x and CO are released into the boundary layer. The intensity of solar radiation is usually also very high during this period and so makes photochemical ozone production more enhanced.

Figure 2.6 the tropics

3 Instruments

Satellite measurements play an important role in scientific studies of the atmosphere. The horizontal and vertical structure of atmospheric trace gas distributions is one of the key elements determining atmospheric composition, atmospheric circulation and climate. For example ozone is a greenhouse gas, is important for OH production in the troposphere and also determines the temperature profile in the stratosphere. As such it is considered as one of the most important trace gases. Therefore it is essential to measure and monitor its distribution and to interpret and understand the measured distribution and changes therein.

New developments in monitoring techniques have stimulated the design of spectrometers, such as GOME and SCIAMACHY, which are potentially able to observe the atmospheric distribution of ozone and a number of other atmospheric trace gases both in the stratosphere and the troposphere. GOME has provided data for comparison with ozone sonde data in this study, and as a result the main operational mode and scientific objectives are described in details below.

3.1 The Global Ozone Monitoring Experiment (GOME)

GOME was launched on the ERS-2 (European Remote Sensing) satellite by the ESA (European Space Agency) in April 1995. It is a grating spectrometer operating from 240 to 790 nm [Burrows, 1988; Burrows, 1993] (i.e. ultraviolet, visible, and near-infrared) with a moderately high spectral resolution (between 240 and 400 nm it is approximately 0.2 nm; between 400 and 790 nm it is approximately 0.4 nm). This wide spectral range allows for the retrieval of the distribution of several trace gases, such as O_3, NO_2, BrO, H_2O, HCHO, SO_2 and OClO

The ERS-2 flies in a sun-synchronous orbit at an altitude of 780 km with a local crossing time (at the equator) of approximately 10.30am local time in a descending mode. The corresponding orbital period is about 100 minutes. With its maximum swath of 960 km across track, GOME can provide complete coverage of the globe at the equator in approximately three days [Burrows et al., 1997].

The main operation mode of GOME is nadir viewing but it is also able to carry out occultation measurements of the sun and the moon so that absolute radiometric calibration, as well as wavelength calibration, is possible.

GOME is as a double spectrograph, which pre-disperses, light at a prism and then produces a spectrum using a set of holographic gratings. A combination of this optical arrangement and the use of array detectors enables the simultaneous observation of the earth's back scattered and reflected spectrum between 240 and 790 nm.

Radiation enters GOME via a scanning mirror, which scans across track with a maximal scanning angle of 31° with respect to the nadir mode. By varying the scan angle the influence of cloud cover on the retrieval of data can be investigated. During each forward scan of 4.5s, GOME scans from east to west and integrate three times1.5s, leading to three ground-pixels 'east', 'nadir', and 'west' ground-pixels. The motion of the scan-mirror is then reversed for 1.5s and a back-scan measurement is taken (see figure 3.1). The back-scan is three times faster than the forward scan, this makes the back-scan ground-pixel three times larger than the forward scan ground-pixels.

The light that enters GOME via the scan-mirror is split into four main spectral channels using prisms and dichroic mirror. The light of each spectral channel is decomposed further by a grating, after which it is focused onto a recticon diode array consisting of 1024 detectable pixels.

3.1.1 GOME Spectral Channels

GOME has four different spectral channels each of which has been chosen to observe different species and different spectral features (see table 3.1).

Channel 1 (240-312 nm): absorption due to the Hartley band of O_3 and NO emission are the dominant features. Channel 2 (309-405 nm): a variety of target species absorb in this region e.g. O_3 (Huggins band), O_4, NO_2, HCHO, SO_2, BrO, ClO, and OClO. Channel 3 (400-605 nm): the target molecules for this region are NO_2, OClO, O_2, O_3 (Chappuis band), O_4 and H_2O. Channel 4 (590-790 nm): the target molecules are O_3 (Chappuis band), NO_3, H_2O and O_2.

The combination of Channels 2 to 4 can be used to make measurements of O_2 and O_4 column amounts, which yields information on radiation penetration depths and cloud top heights. Also the back scattered light provides information about atmospheric aerosol and polar stratospheric clouds.

Species	**Retrievable Quantity**[1]	**Wavelength (nm)**
O_3	Profile (S,T)	240-360; 410-680
O_2	Column (S,T)	690, 760
O_4	Column (T)	360, 380, 477, 516, 630
H_2O	Column (S,T)	500-790
HCHO	Column (T)[2]	310-360
SO_2	Column (T)[2]	290-310
NO	Column (S,M)	255-280
NO_2	Column (S,T)	300-600
ClO	Column (S)[3]	290-320
OClO	Column (S)[3]	320-420
BrO	Column (S)	310-380

Table 3.1: Quantities retrieved from GOME observations

(1) S = stratosphere; T = troposphere; M = mesosphere

(2) Observable in regions with relatively high concentrations

(3) Observable in perturbed "O_3 hole" conditions

(4) Observable in twilight regions

3.1.2 The Scientific Objectives of GOME

As indicated earlier, a primary scientific aim of GOME is the measurement of total column amounts of those gases, which absorb between 240 and 790 nm, in the special case of O_3 (and possibly NO_2, SO_2 and aerosols). It is also intended to derive some gases which in a clean unperturbed atmosphere have very low concentrations, but which can achieve moderately high concentrations under certain circumstances e.g. SO_2 or HCHO in a polluted troposphere. OClO in the lower stratosphere during 'ozone hole' episodes can also be measured. In addition to the known absorptions due to the gases listed in table 3.1, other structured features are known to be present in the part of the atmospheric spectrum that will be observed by GOME.

3.1.3 Cloud Information

GOME [Brewer et al., 1973] observes both the troposphere and the stratosphere, and in cloudy situations it is impossible for GOME to detect the exact influence of trace gases near the ground under the cloud layer because tropospheric columns are obtained by subtracting the above-cloud stratospheric amount from the total amount with a reflectivity < 0.1[Richter, 1997].

The penetration depth of light in the atmosphere is determined from GOME data from observations of O_2 and O_4 (a dimer of O_2) absorption. The combination of the O_2/O_4 penetration depth and the measurement of the wavelength dependence of albedo enable the presence of clouds to be detected and cloud top heights to be estimated. The absorption band allows for the estimation of multiple scattering in the troposphere and also retrieval of information about the extent of cloud cover.

Polarisation detectors are used to increase the spatial resolution of the cloud measurements.

3.1.4 Observations of Aerosol Distributions

1) Stratospheric Aerosol and Polar Stratospheric Clouds

It is intended to use GOME to detect stratospheric aerosols and polar stratospheric clouds (PSCs) – the retrievable product being total optical thickness. The approach is still being investigated but has been demonstrated for balloon limb observations. It requires first the determination of the phase function of the aerosol scattering efficiency at several wavelengths. Subsequently a model of this parameter is used in a data fitting procedure to identify a compatible size distribution.

2) Tropospheric Aerosol

Although it is intended to use GOME to monitor tropospheric haze, this is difficult because of the strong influence of Rayleigh scattering in the troposphere. Fortunately it is extremely time dependant. This should allow the high spectral resolution of GOME instrument, combined with its spatial resolution, to be used to study image contrasts and hence to characterise the nature of haze in terms of natural phenomena. The same reasoning applies to forest fires, which release large quantities of soot to which, for decades, the blue moon phenomenon has been attributed.

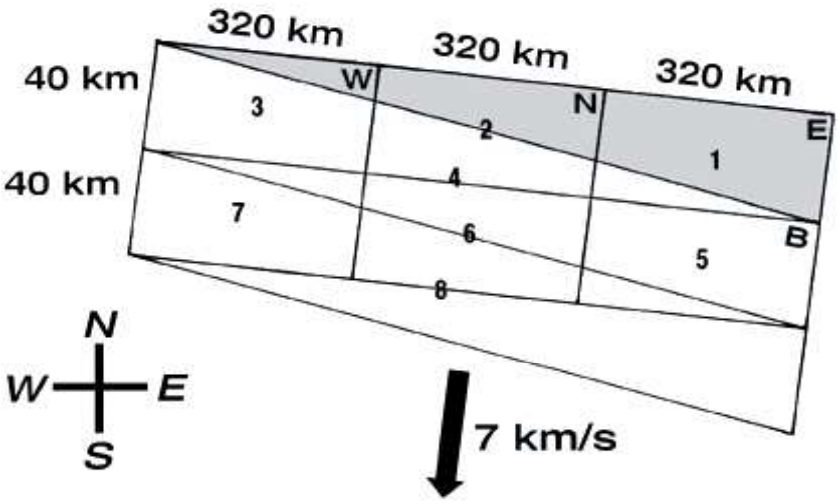

Figure 3.1: GOME Scan Geometry in Nadir Viewing

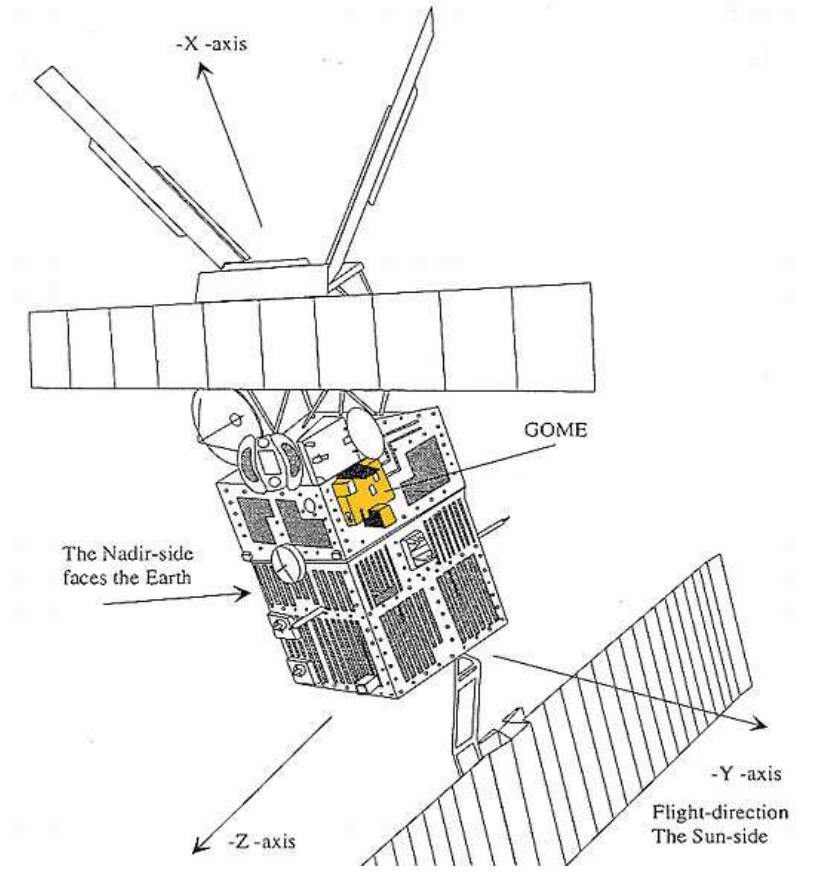

Figure 3.2 ERS-2-Satellite with GOME onboard

3.2 The FUll Retrieval Method [FURM] Algorithm

The Full Retrieval Method (FURM) [Rozanov et al., 1997] was developed at the Institute of Remote sensing, University of Bremen to enable the retrieval of height resolved ozone information from GOME sun normalized spectra.
It uses temperature dependence absorption in the Hartley - Huggins bands of ozone [Richter, 1995]. The GOME instrument is suitable for the detection of the absorption features variation due to temperature changes.

The FURM algorithm uses spectral information from Channel 1a (240-308 nm, 12s integration time) and Channel 2 (316-400 nm, 1.5s integration time). The ground coverage of Channel 1a corresponds to a surface area of 960 x 80 km^2, and that of Channel 2 to a smaller surface area of 320 x 40 km^2. In order to obtain an approximately identical surface coverage in each spectral GOME channel, the channel 2 spectrum is co-added from the three spectra available in the across-track scan direction, i.e. east, nadir, and west ground pixels. Both Channel 1A and 2 spectra are fitted simultaneously in FURM. The broad spectral range as currently used in FURM is required in order to derive both stratospheric and tropospheric ozone.

The fitting parameters in FURM are the ozone column densities at 61 equidistant levels between 0 and 60 km, the height integrated Rayleigh scattering and aerosol coefficient, total column of NO_2 and the scaling factor of the Ring spectrum.
Certain assumptions about the state of the atmosphere and the ground have to be made to restrain the number of possible solutions of the retrieval. As a first time guess, the climatology of the atmosphere from the MPI-Mainz for chemical 2-D

model is used [Brühl et al., 1991], which consists of height dependent trace gas concentration, pressure and temperature for different latitudes and months.

Aerosol scattering and absorption coefficients are taken from the LOWTRAN database [Kneizys et al., 1988].

Calculated solar zenith angle dependent Ring reference spectra due to Raman scattering on N_2 and O_2 molecules are included in the radiative transfer model [Vountas, 1997]. The Ring effect is one of the error sources that affect measurements and for which a correction is needed. It was first discovered by Ring, that spectra of sunlight scattered in the atmosphere undergo a washing out effect (e.g., filling in of the fraunhofer lines), which could not be explained by theory.

The O_4 absorption band was used to detect cloud information, such as the cloud top height and the cloud cover.

The two major parts of the FURM are:

3.2.1 A forward Model: Based on the radiative transfer model (RTM) GOMETRAN [Rozanov et al., 1997] which calculates the top of atmosphere (TOA) radiance and the weighting functions for a given state of the atmosphere as defined by:

- the Ozone vertical distribution
- trace gas distribution
- surface albedo,
- aerosol scenario

The weighting functions describe the response of the radiance to small deviations of the atmospheric parameters from a given atmospheric state. They are the partial derivatives of the forward model with respect to the atmospheric parameter.

These derivatives are usually calculated by means of numerical perturbation schemes. The finite differences method allows the direct, quasi-analytical computation of the weighting functions, which reduces drastically the computation time [Rozanov et al., 1998].

3.2.2 An Inversion Scheme: matches in iterative steps the calculated TOA radiance and the measured GOME radiance by modifying model atmospheric parameters such as the vertical distribution of ozone using an appropriate weighting function as defined by GOMETRAN. Figure 3.3 shows the steps involved in the iteration steps.

Two alternative inversion techniques can be employed in FURM. They are based on the optimal estimation approach and the eigenvector method. The latter is however preferred since it yields superior results [de Beek, 1997].

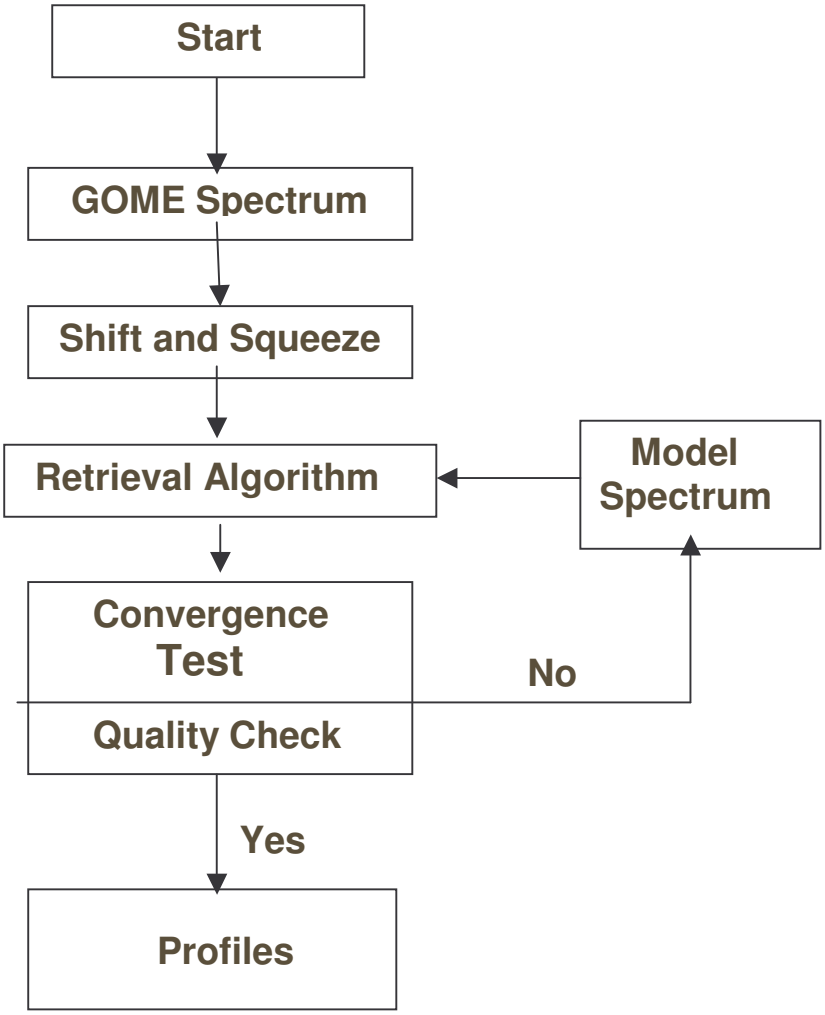

Figure 3.3 : The FURM scheme

The first step in the scheme is the reading of the measured spectrum and the model spectrum in the wavelength region between 290 and 307 nm.

Afterwards a shift and squeeze routine is performed. This is necessary because GOME measures the solar radiance and irradiance at two different locations and this might lead to a shift between the two spectra. Also the two parameters are subject to small Doppler shift as a result of the relative motion between the sun and the satellite. In order to correct for any artificial spectra that might occur as a result of these in the sun normalized radiance, the shift and squeeze routine is

performed to align the two spectra. This approach is, however only suitable for small spectral windows. The GOME TOA radiance ranging from 290 – 340 nm is therefore divided into three spectral windows of 290 – 307 nm, 316 – 325 nm, 325 – 340 nm, for which independent shift and squeezes are applied.

The ozone profile is afterwards derived by implementing the equation below [Rodgers, 1976].

$$X_{n+1} = X_a + (K_n^T S_y^{-1} K_n + S_a^{-1})^{-1} K_n^T S_y^{-1} [(y - y_n) - K_n (X_a - X_n)] \quad 3.1$$

where,

X_{n+1} = fit / profile result

K_n = Weighting functions

S_a = apriori covariance matrix

X_a = apriori profile

S_y = measurement error covariance matrix

y = reflectance

n = iteration steps

The solution for the above equation starts with a first guess profile X_1, and proceeds through n iteration steps. When the profile result is achieved, comparing the profile result to a chi-square carries out a convergence test,

$$\chi^2 = (y_{n-1} - y_n)^T s_y^{-1} (y_{n-1} - y_n) << m \quad 3.2$$

where,

χ^2 = Value of actual & previous model spectra and

m = number of spectral points.

If m is an order of magnitude smaller than χ^2, then convergence has occurred.

A quality check is finally carried out to determine whether the profile result corresponds to the measurement spectrum within measurement error from the relation,

$$\chi^2 = (y - y_{n+1})^T S_y^{-1} (y - y_{n+1}) \approx m \qquad 3.3$$

If the above condition is satisfied, the profile is derived; otherwise the whole process shall be repeated until the conditions are satisfied.

3.3 SONDE Measurements

Ozone sondes used in this work are from SHADOZ (Southern Hemisphere ADditional OZonesondes) for the tropics and the DWD (Deutscher Wetterdienst) for the northern hemisphere.

In 1998 NASA's Goddard Space Flight Center (GSFC), together with NOAA's Climate Monitoring and Diagnostics Laboratory (CMDL) and international sponsors established the SHADOZ project to address the gap in tropical ozonesonde coverage (Thompson et al., 2002a,b). SHADOZ augments launches at selected sites and provides a public archive of ozonesonde and radiosonde data from eleven tropical and subtropical southern hemisphere operational ground stations (see table 3.2). The first SHADOZ site in the tropical northern latitudes (Paramaribo, Surinam) joined in 2000. Data are available to the community at the website maintained at NASA/Goddar (http://croc.gsfc.nasa.gov/shadoz/).

Current sampling at all stations is once-per-week or twice a month, usually but not always, mid-week. They usually measure from the ground level to about 40 km altitude. At this altitude the balloon bursts and the sonde falls down. Balloon-borne ozonesondes are coupled with a meteorological radiosonde for data telemetry transmitting air pressure and temperature, relative humidity, and ozone to a ground receiving station. All stations are using electrochemical concentration cell (ECC) ozonesondes. Radiosonde packages vary from station to station and determine the recording frequency and raw data format.

Station	Location	Co-I/Affiliation	Operational time
Ascention Is	8S,14W	F.J.Schmidlin NASA / WFF	1990 – 92; 1997– present
America samoa	14S,171 W	S.J.Oltmans NOAA/CMDL	1995 – present
San Cristobal Equator	1S, 90W	S.J.Oltmans NOAA/ CMDL	1999 – present
Fiji Is	18s, 178E	S.J.Oltmans NOAA CMDL	1996 – present
Watukosek, Indonesia	7,57S, 112.65E	T. Ogawa NASDA,Japan	1993 – present
Nairobi, Kenya	1S, 37E	B. Hoegger, B.Calpini Meteo	1996 – present
Malindi, Kenya	3S, 40E	G.Laneve Univ. Rome, Italy	1999 – present
Natal, Brazil	5S, 35W	V.W.J.H.Kirchof f INPE,Brazil	1978 – present
LaReunion France	21S, 55E	F.Posny Univ. deLa Reunion	1992 – present
Irene , S. Africa	26S, 28E	G.J.R. Coetzee SAWS	1990 – 93 1998 – present
Tahiti Is	18S, 149W	S.J.Oltmans NOAA/ CMDL	1995 –1999
Paramaribo Surinam	5N, 55W	H. Keldr KNMI, Netherlands	1999 – present

Table 3.2 SHADOZ tropical and subtropical ozonesonde stations. Only data from 1998 onward is in the SHADOZ archive

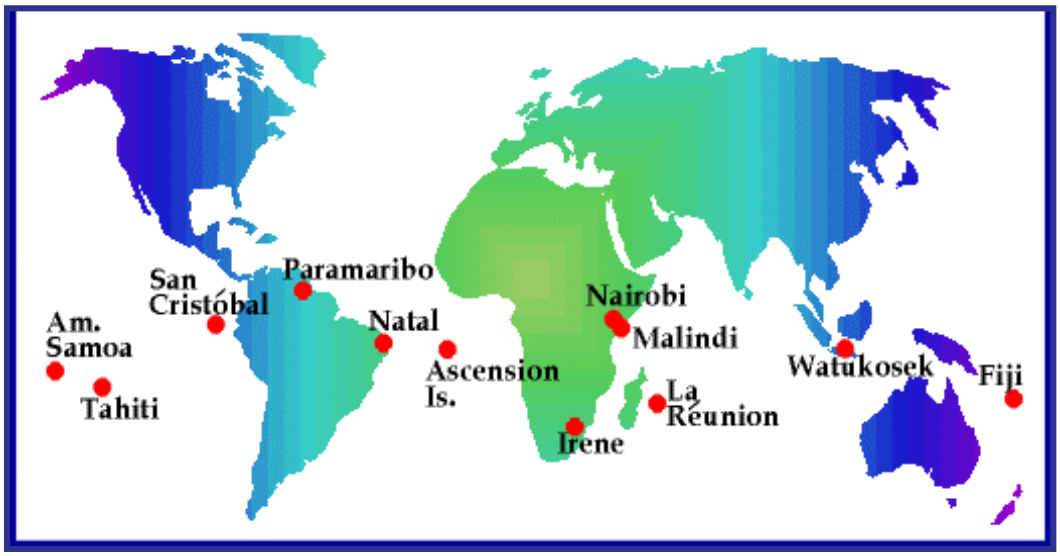

Figure 3.4 Map of SHADOZ stations. There are 12 stations currently operating; Tahiti ceased launches at the end of 1999 [http://croc.gsfc.nasa.gov/shadoz/Sites2.html]

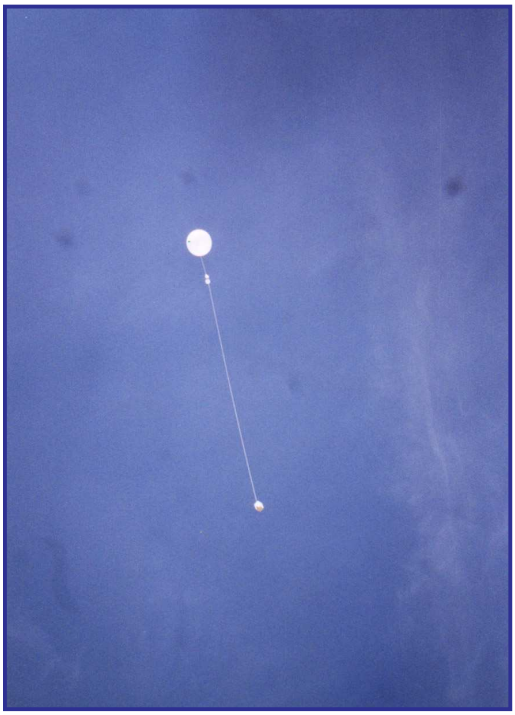

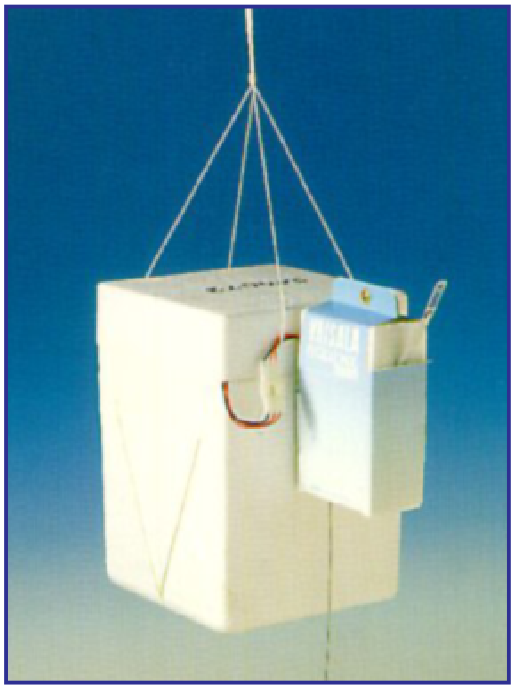

Figure 3.5 a balloon launch carrying the ozone sonde instrument is shown in the first picture, while the second picture shows the instrument

4 Results and Discussion

From GOME level-2 data, ground pixels were extracted from two different locations and implemented in the FURM algorithm so as to derive the tropospheric ozone vertical column.

4.1 Watukosek [Lat 7.57S, Long 112.65E]

During the burning season of 1997, wildfire burnt extensively in Indonesia as a result of the EL-Niño related long dry season experienced.

El-Niño is the local warming of the sea surface temperature (SST) of the entire equatorial region of the central and eastern Pacific Ocean. During an El Niño event, the trade winds weaken and warm; nutrient-poor water occupies the entire tropical Pacific Ocean. Heavy rains that are tied to the warm water move into the central Pacific Ocean and cause drought in Indonesia and Australia.

It is referred to as ENSO (El-Niño Southern Oscillation) when accompanied by an east-west balancing movement of air masses between the pacific and the Indo – Australian areas. El-Niño is the oceanic component, while Southern Oscillation is the atmospheric component.

The opposite phase of El-Niño is the La-Niña, where the trade winds are stronger and cold, nutrient-rich water occupies much of the tropical Pacific Ocean. Most of the precipication occurs in the western tropical Pacific Ocean, so rain is abundant over Indonesia.

1997 was a year of an El-Niño event, while 1998 represents a La-Niña year.

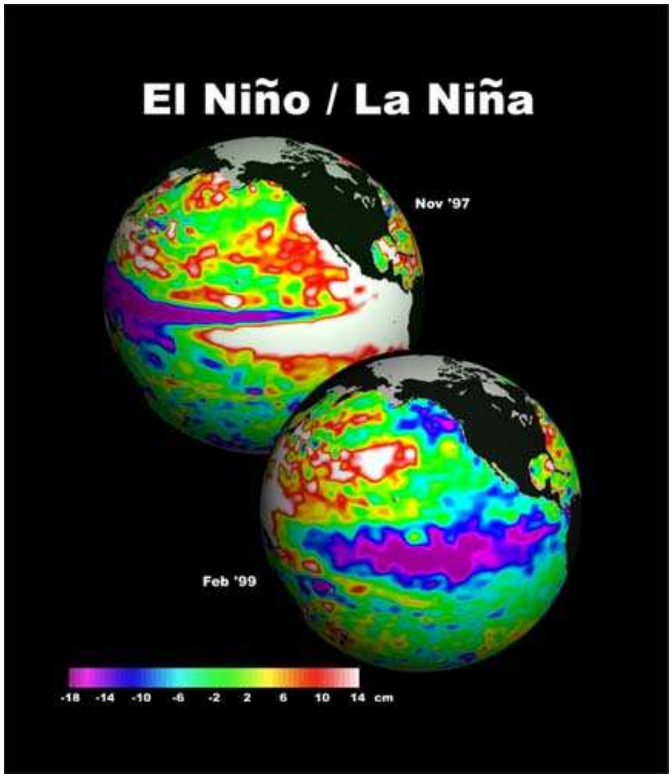

Figure 4.1 La-Niña and El-Niño [Courtesy NASA]

As a result of this, fire burnt uncontrollably leading to high emission of atmospheric pollutants.

In order to investigate the effect of these pollutants on tropospheric ozone production, nadir ground pixels were extracted from selected GOME orbits for this geolocation or near geolocation for 1997 that is about 500 km to 1000 km radius.

1998 was also analysed as burning again resumed, however to a much lower extent as compared to 1997. This analysis is necessary so as to investigate the intensity of tropospheric ozone production under these two different periods of El-Niño and LA-Niña.

Figure 4.2 The green arrow shows the location for Watukosek

4.1.1 Extraction Procedure

GOME orbits were selected for those days sonde measurement were available.

After the selection, nadir ground pixels were systematically extracted with a defined programme.

Then the implementation for the selected pixels was made separately in the FURM algorithm. Here properties such as the cloud top height, exact geolocation, cloud fraction, scan solar zenith angle and effective albedo for each pixel were defined.

This information was later compiled and the ozone vertical column for sonde, GOME as well as that of apriori was derived.

In calculating the tropospheric ozone vertical column, the tropopause height was defined using the sonde ozone profile for each extraction. In the tropics the tropopause height was quite stable at around 17 km, this made the calculation much easier as a different tropopause height do not have to be defined in each case. The tropospheric ozone amount was then determined by transferring the data into molecules/cm^3, taking into account the non-linearity of pressure and

temperature, multiplying with the thickness of the layers and finally integrating up to the calculated heights of the tropopause.

Shown in figure 4.3 is an ozone vertical profile for a GOME ground-pixel extracted for the 13th of August 1997. The black curve indicates the sonde profile, while the green and the pink curves are for the FURM and apriori profiles respectively.

.

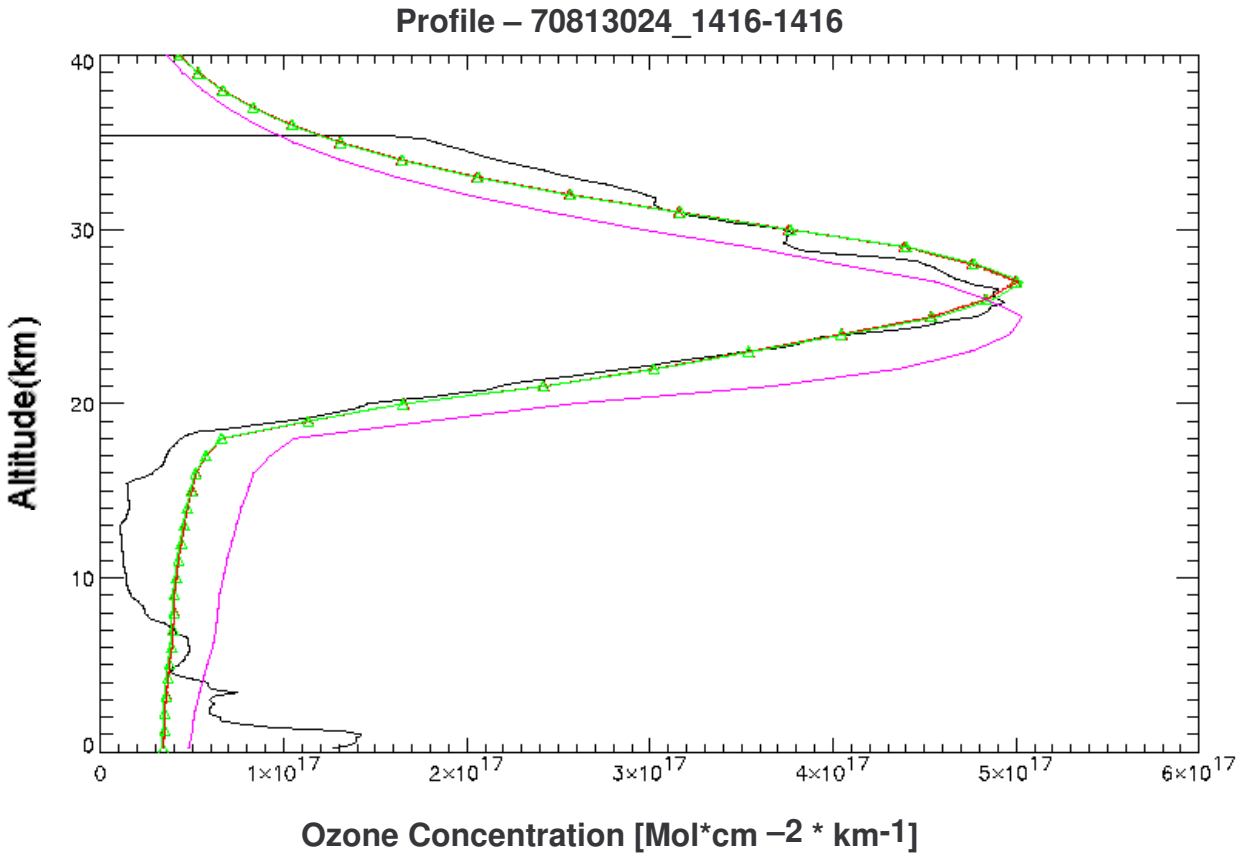

Figure 4.3 Ozone vertical profiles for a GOME ground pixel extracted for the 13th of August 1997. The black, green and pink curves indicate the sonde, FURM and apriori profiles respectively

The result of the derived tropospheric ozone vertical column for 1997 to 1998 for sonde (red curve) and FURM (black curve) plotted as a function of time of the year (months) is shown in figure 4.4.

Both curves show a good agreement in trend. There is a similarity in the seasonal distribution in both cases, with a background concentration (10 – 25DU) of ozone recorded between January and March 1997. Retrieval was not made between April and July, as there was no available sonde measurement. However, from August to November a rather higher value was recorded (30 – 55DU), with the maximum value (sonde, 55DU and FURM, 51DU) observed in the month of October.

This peak value at this period is an attribution of the emissions from biomass burning activities, which eventually lead to photochemical production of tropospheric ozone (see section 2.4). The El-Niño events also contributed to the high value because of the high drought experienced. This high value however decreases towards December as the effect of the emission becomes less intense.

In 1998, a generally better agreement was achieved between the two results. Averagely low ozone value (15 – 26DU) was recorded almost all the year round with the exception of the months of October and November (28 –35DU). As was the case for 1997, maximum ozone value (sonde, 35DU and FURM 33DU) was also recorded at around October. This is also an evidence of photochemical production of ozone from biomass burning emissions, however much lower to the maximum recorded in 1997 because of the less intensity of the 1998 burning activities. We shall recall that 1998 is of course a La-Niña year.

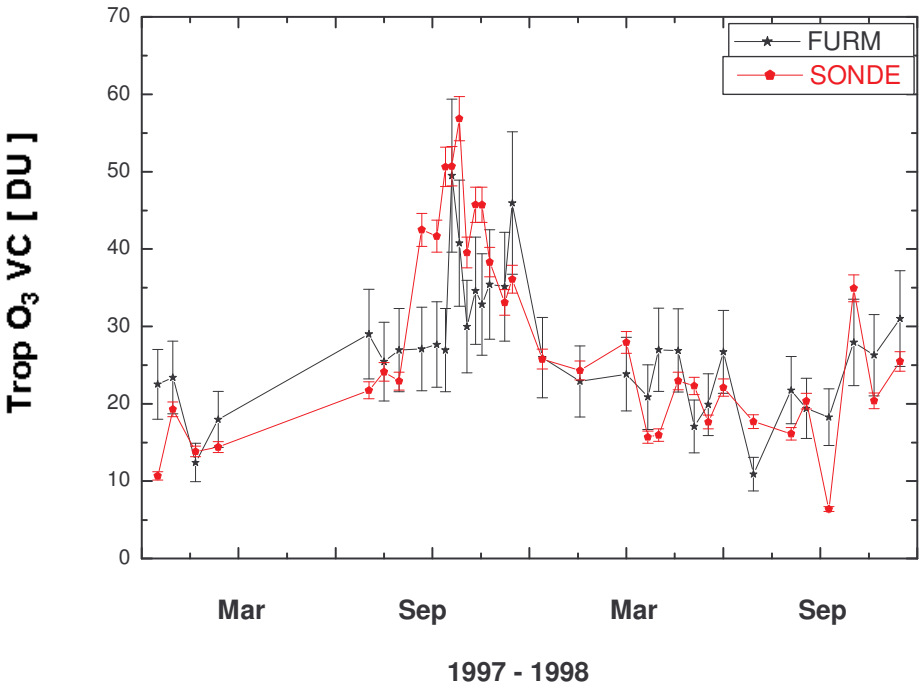

Figure 4.4 Tropospheric ozone vertical column from sonde (red curve) and FURM (black curve) plotted as a function of time (months).

The relationship between both results is shown in figure 4.5 where tropospheric O_3 vertical column from sonde was plotted as a function of that as derived from FURM. A good positive correlation could be seen between the two results with $r = 0.74$.

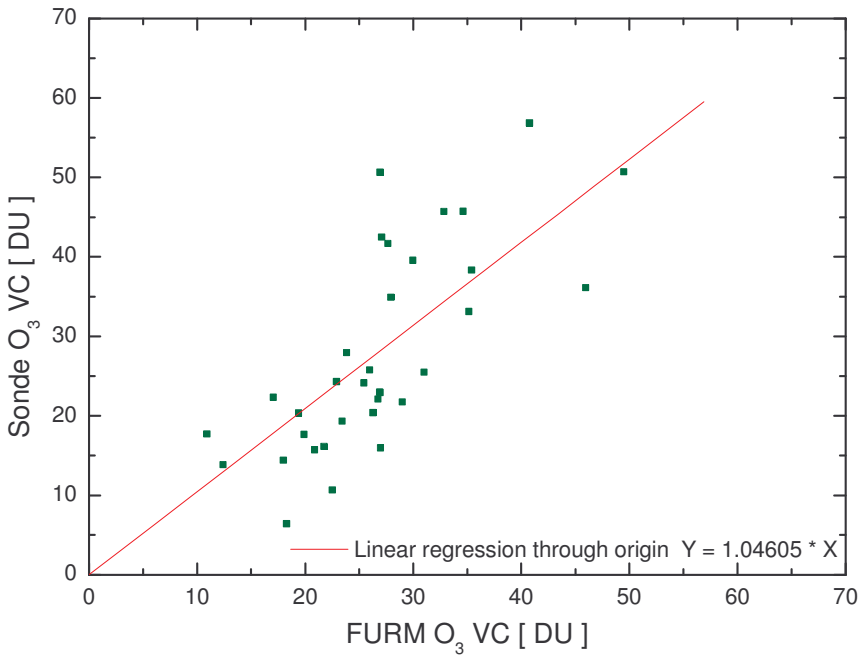

Figure 4.5 Sonde tropospheric O_3 vertical column versus FURM tropospheric O_3 vertical column

Generally the differences in the sonde and FURM measurements fall within the 10% error allowed for the FURM. This implies a good agreement in measurements. Despite the good agreement, however larger deviations of about 20% were observed between August and September, 1997. This could be due to differences in geolocation in some instances.

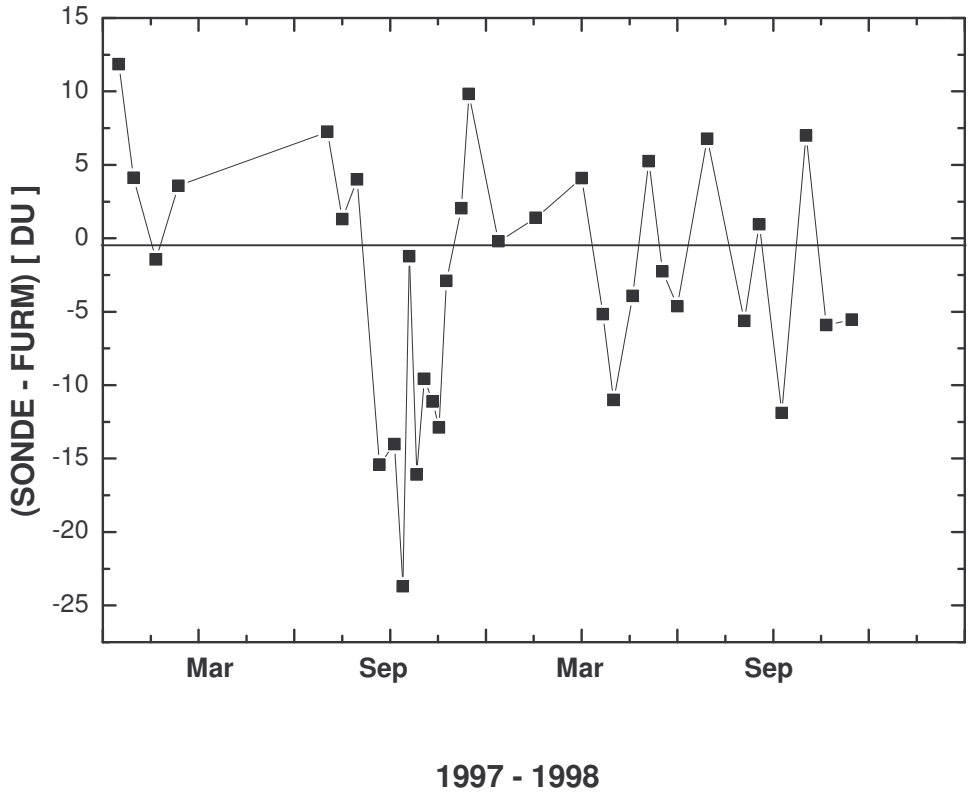

Figure 4.6 (SONDE – FURM) DU as a function of time (months)

Another source of error could have been cloud cover and the effect of these (cloud fraction and cloud top height) on the result was investigated. Cloud fraction and cloud top height was derived using the O_4 absorption band. In figure 4.7 and 4.8 are plots of the (sonde - FURM) DU as functions of the cloud fraction and the cloud top height respectively.

Very cloudy areas (~ 70%) show a good agreement between sonde and FURM (figure 4.7), while moderately cloudy areas (~ 30 – 40%) also show good agreement. However, the highest deviation was noticed in less cloudy scenarios. The same can also be said of the cloud top height (figure 4.8), as the highest deviation (~ 25 DU) was again recorded in low cloud scenario.

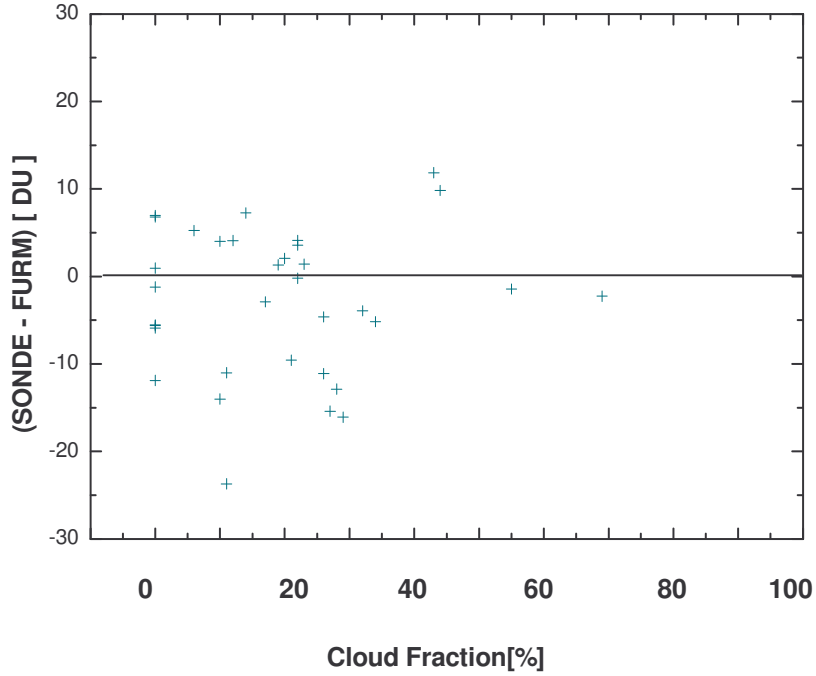

Figure 4.7 (SONDE – FURM) O_3 vertical column as a function of cloud fraction

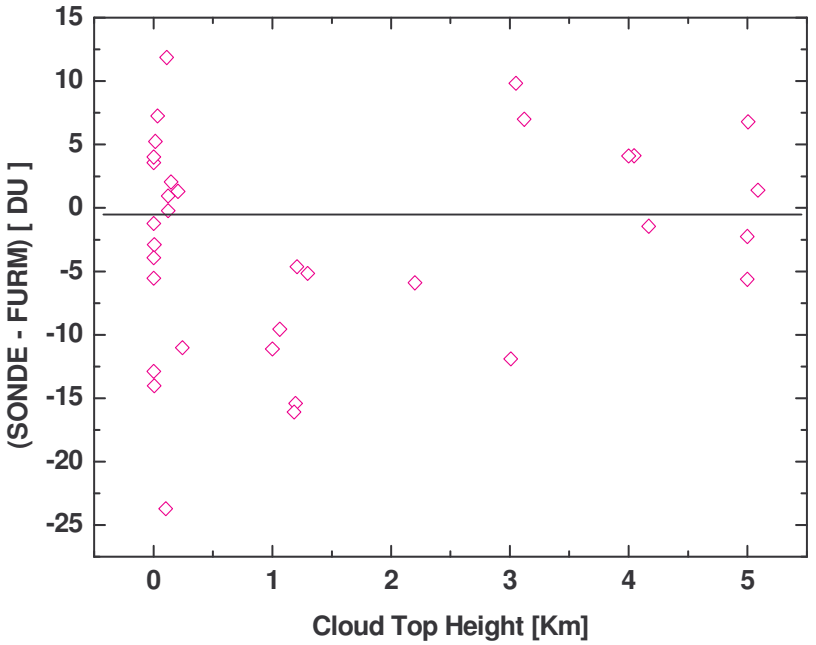

Figure 4.8 (SONDE – FURM) O_3 vertical column as a function of the cloud top height

4.2 Hohenpeissenberg [Lat 48N, Long 11E]

Aside biomass burning emissions, emissions from urban related pollution also play vital roles in the photochemical production of tropospheric ozone (see section 2.4). In view of this, Hohenpeissenberg a location in the northern hemisphere (an urban polluted area) was also analysed. This analysis will help to determine; firstly, the effect of urban pollution on tropospheric ozone production; secondly, make viable comparison between tropospheric ozone production from biomass burning emissions in the tropics (in relation to El-Niño and La-Niña events) and urban pollution in the northern hemisphere; and lastly – investigate the retrieval efficiency of FURM in the two locations.

Figure 4.9 the red spot in the diagram indicates the location of Hohenpeissenberg

4.2.1 Extraction Procedure

GOME orbits were selected for days with corresponding sonde launching for 1997, from where nadir pixels were extracted and implemented in FURM to derive the ozone vertical profile.

There are, however major differences that makes the calculation of the tropospheric ozone vertical column in the northern hemisphere (NH) differ from the tropics.

1) Tropopause height: - The tropopause height is quite lower and in most cases, varying from between 7 km to about 15 km altitude. In order to reduce stratospheric influence, tropopause height was defined for each extracted pixels with respect to the sonde vertical O_3 profile.
2) Meteorological conditions
3) Sonde measurements: - most sonde stations are located in the NH – this makes a lot more data available for comparison
4) Cloud cover is much higher than in the tropics, so as a result a higher albedo (see section 1.3) is prevalent.

After taking all this into consideration, the profiles were finally derived and the tropospheric ozone vertical column calculated. In figure 4.10 is an example of the derived vertical profile of ozone for a GOME ground pixels extracted for the 27th of August 1997. The green curve indicates the FURM profile from GOME data, black curve indicates the sonde profile and the pink curve is for the apriori profile. The tropopause height is evident from figure 4.10 at about 12km altitude.

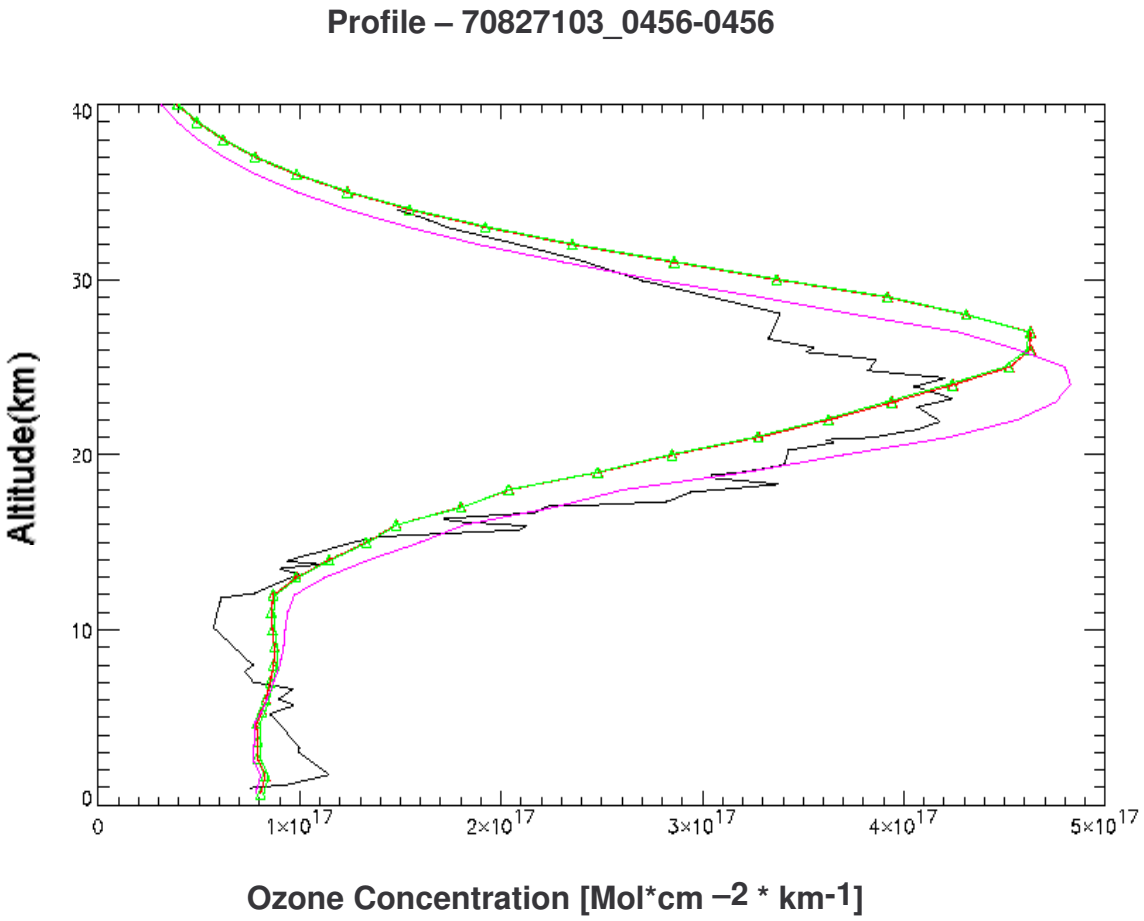

Figure 4.10 Ozone vertical profile for a GOME ground pixel extracted for the 27th of August 1997. Black curve indicates the sonde profile, green is for the FURM profile and the pink is the aprioiri profile

The calculated ozone vertical columns for both the sonde and FURM were plotted as a function of time (months) in figure 4.11. The figure indicates an overestimated ozone value in the late winter towards the early spring months (January to April) by FURM, while there is a much better agreement in the summer months. The summer maximum possibly as a result of ozone production from anthropogenic emissions observed from GOME data is consistent with the trend from sonde observations.

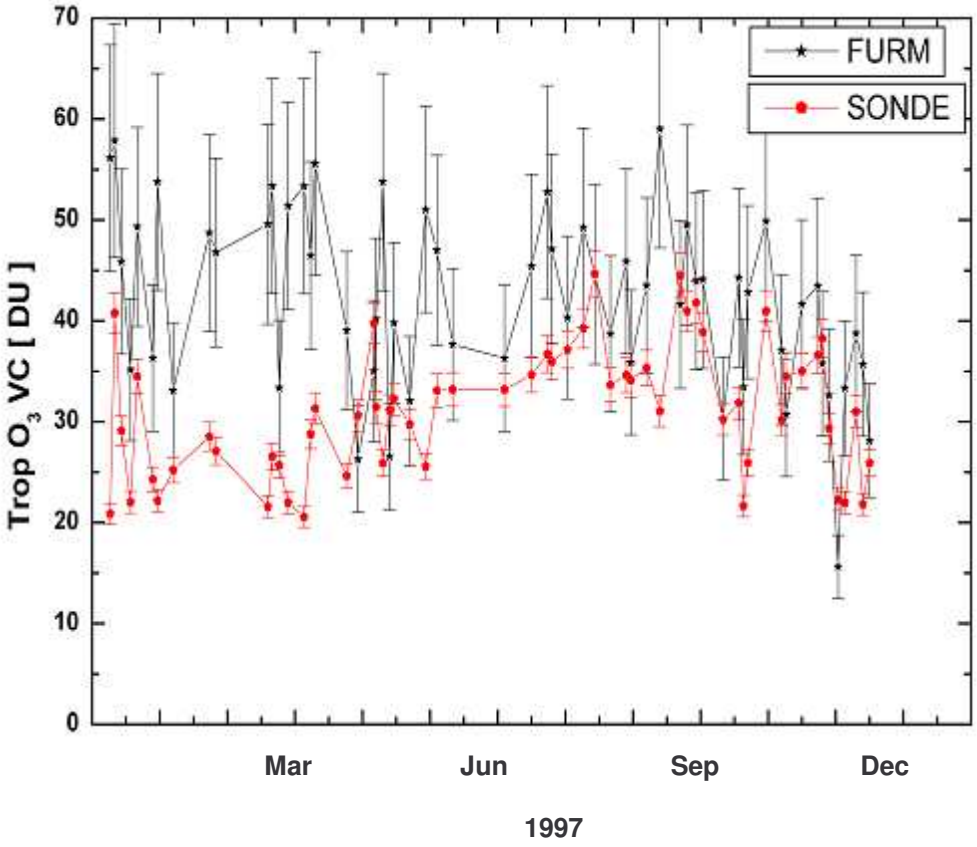

Figure 4.11 Tropospheric ozone vertical column for sonde (black curve) and sonde (red) curve as a function of time (1997)

Because of this late winter and spring maximum, 1998 was also investigated for the same location in order to determine if the same maximum will reoccur at the same period. Figure 4.12 shows a similar result to the previous result for 1997, with the same late winter and spring maximum. The result also indicates a much better agreement in the summer and early winter months.

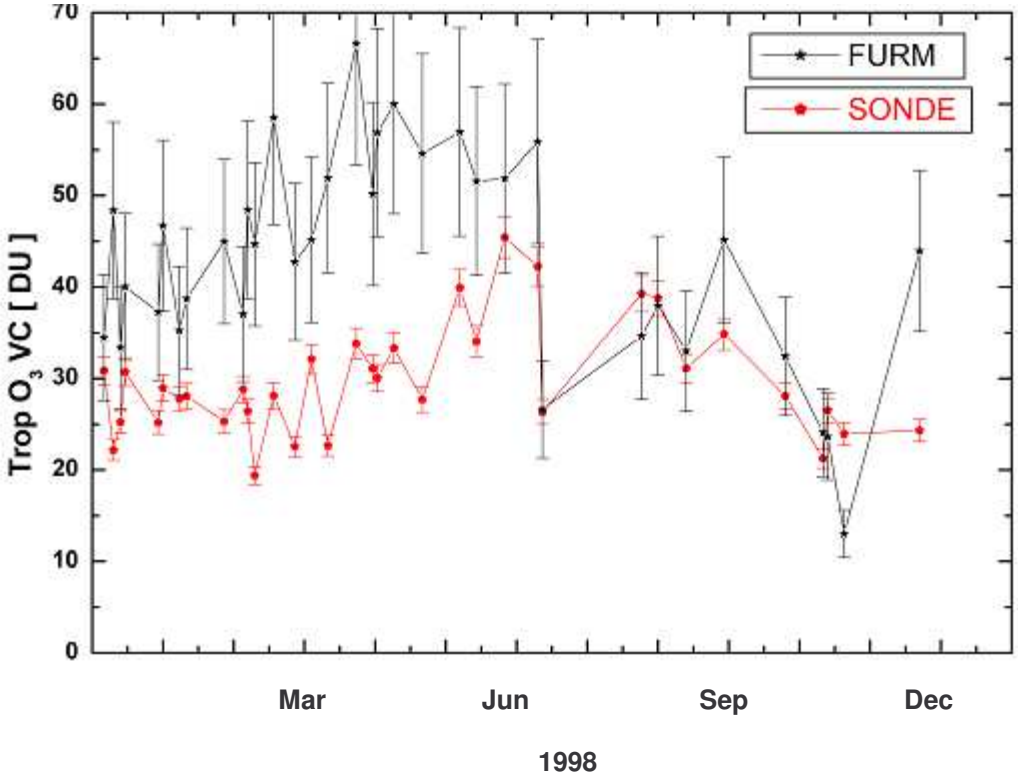

Figure 4.12 Tropospheric ozone vertical column plotted as a function of time (1998). Sonde is shown in red and FURM in black

The large discrepancies at this time could be as a result of the less instability in the tropopause height in the late winter and spring months. These could have allowed the tropospheric ozone to be infiltrated by downward transport of stratospheric ozone. In order to investigate this, a comparison was made between the total ozone vertical column derived from GOME data and the Total Ozone Monitoring Spectroscopy (TOMS) measurements from January 1997 to April 1998. As sonde measurement is only applicable up to between 33 km to 40 km where the balloon eventually burst, it is not possible for the sonde to determine the total ozone vertical column. Figure 4.13 shows a very good agreement in the total ozone vertical column from GOME and TOMS, buttressing the fact that

stratospheric intrusion could have been a major factor responsible for the tropospheric ozone spring maximum recorded in both 1997 and 1998.

The FURM algorithm has defined the tropopause height for each particular pixel extracted using the sonde ozone profile from which the tropospheric ozone vertical column was calculated. This method of determining the tropopause height, however might not be too effective in properly separating the stratospheric ozone from the tropospheric ozone, especially in the spring months.

The large discrepancies could also be as a result of double or multiple cloud layers, which could have lead to multiple scattering between these two or multiple layers. This makes it rather difficult for GOME to give accurate information about tropospheric ozone in this region under such situations. In figures 4.14 and 4.15 are plots of the difference in the tropospheric ozone sonde measurement and FURM for both 1997 and 1998 as a function of the cloud fraction and cloud top height respectively.

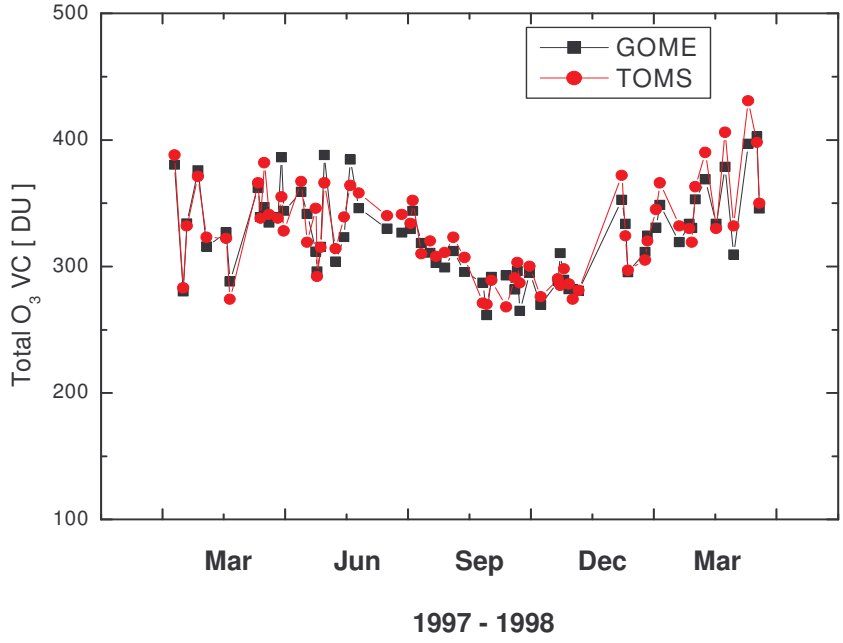

Figure 4.13 Total ozone vertical column from GOME and TOMS, January 1997 – April 1998

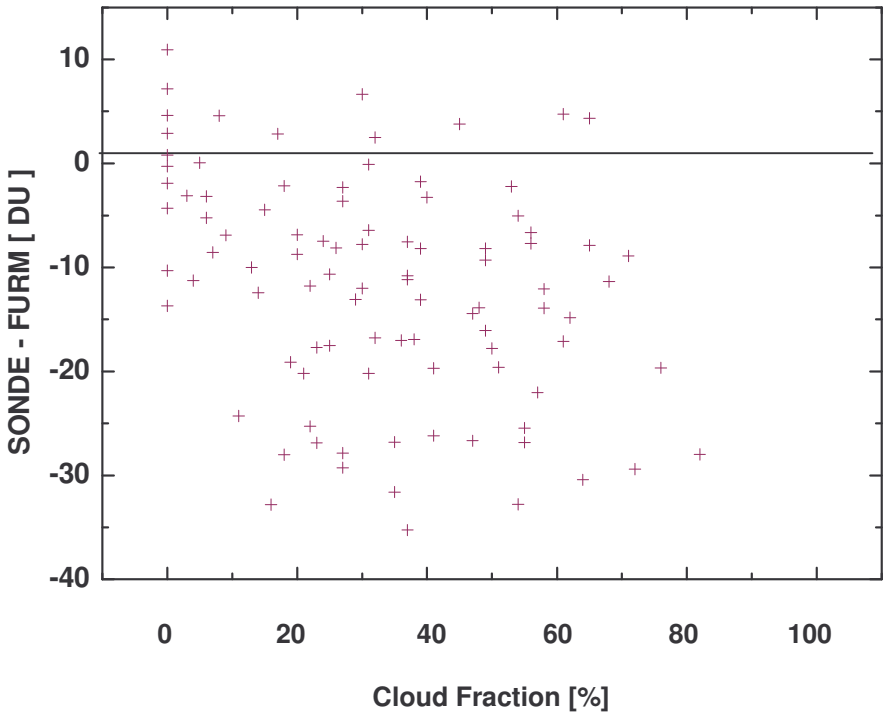

Figure 4.14 (SONDE – FURM) O_3 VC as a function of cloud fraction

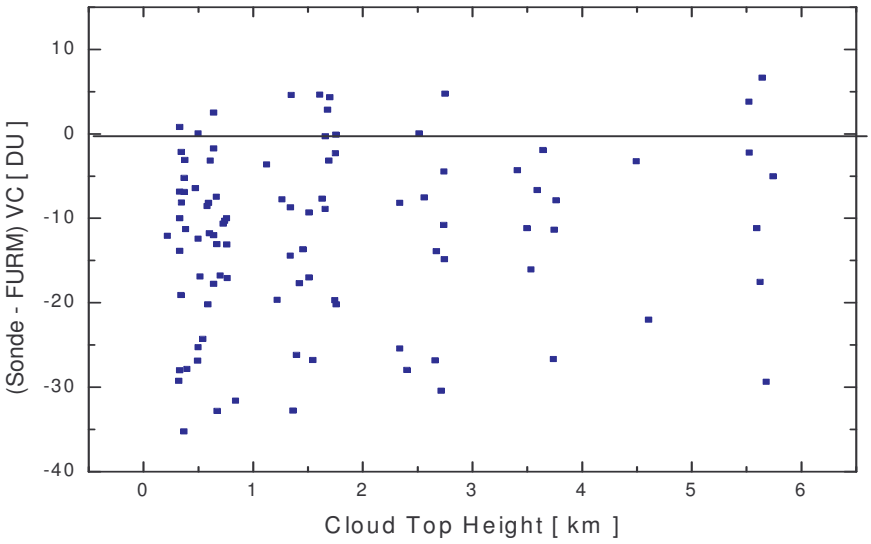

Figure 4.15 (Sonde – FURM) vertical column as a function of cloud top height

Cloud cover looks to have played some roles in the large deviations as shown in figures 4.14 and 4.15. Multiple-scattering which could occur as a result of double of multiple cloud coverage could be the cause for this as the deviations are more pronounced in spring when there are more cloud presence in the northern hemisphere.

4.3 Comparison between Apriori, FURM and Sonde for both Watukosek and Hohenpeissenberg

As apriori information was derived using the MPI-Mainz for chemical 2D model. As a means to further analyse the tropospheric ozone retrieval efficiency of FURM comparison was made between apriori, FURM and sonde for Watukosek (figure 4.16), and Hohenpeissenberg (figure 4.17).

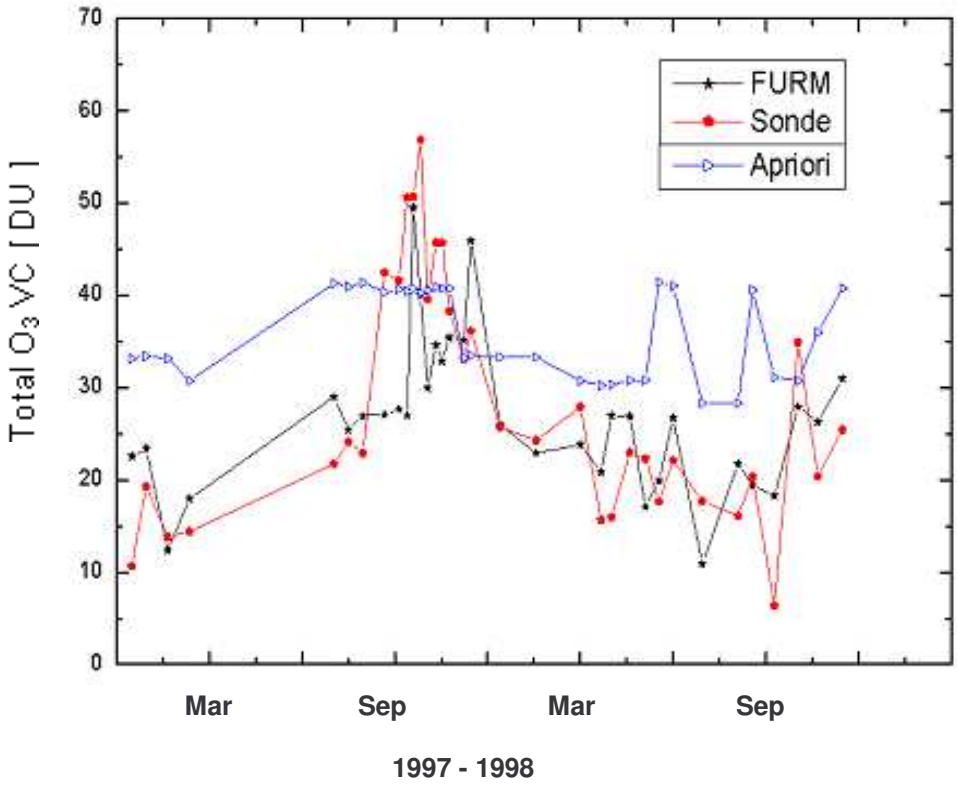

Figure 4.16 Apriori, sonde and FURM tropospheric ozone vertical column (Watukosek)

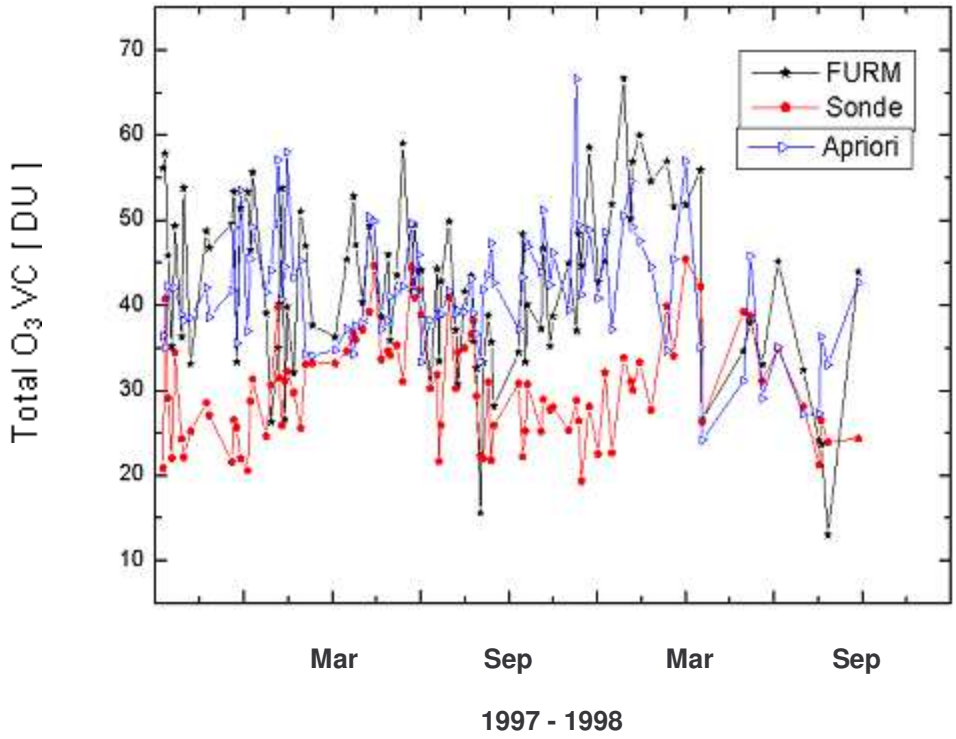

Figure 4.17 Apriori, sonde and FURM tropospheric ozone vertical column (Hohenpeissenberg)

The two figures suggest that FURM seems to work well in the tropics where the result could be seen to be different from the apriori result. However, the northern hemisphere shows a similarity in the two curves (FURM and apriori).

4.4 Comparison between the Northern Hemisphere and the Tropics

This section looks into the major differences between the result derived for the tropics (Watukosek) and the northern hemisphere station of Hohenpeissenberg.

This comparison is necessary in order to investigate the difference/s in the photochemical production of tropospheric ozone from biomass burning emissions (section 2.3) and urban pollution emissions (section 2.2).

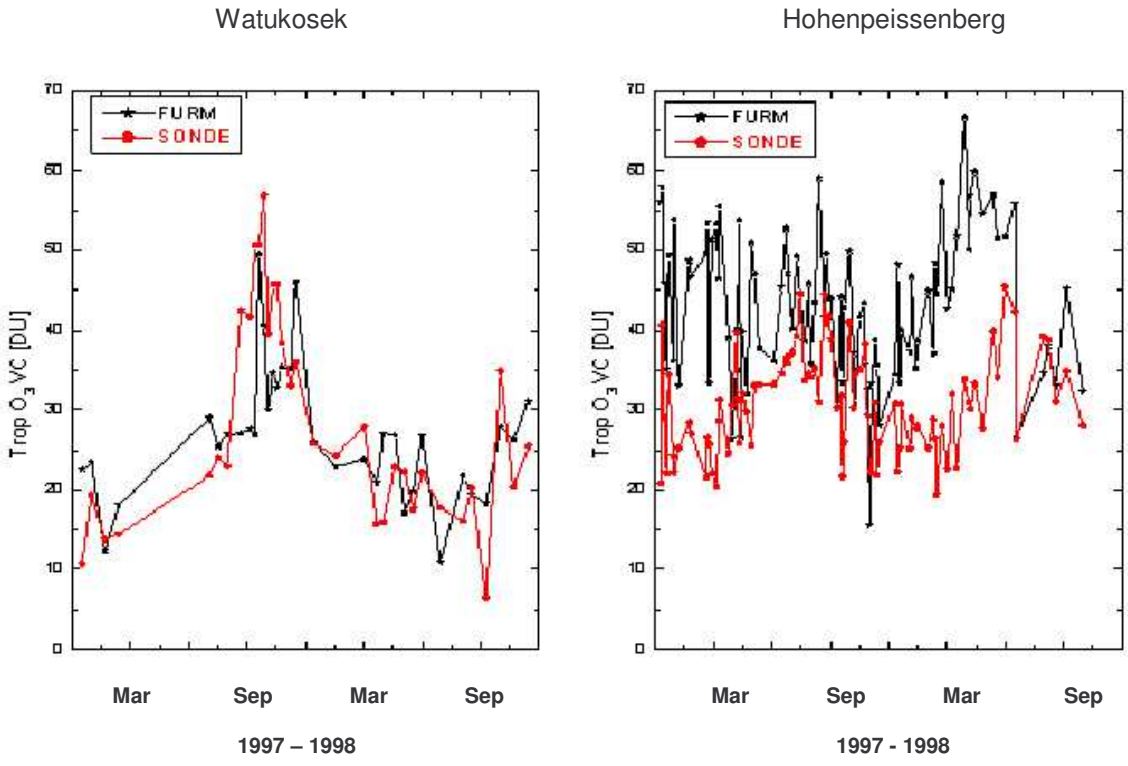

Figure 4.18 Tropospheric ozone vertical column for Watukosek and Hohenpeissenberg

On the left hand side of figure 4.18 is the result from Watukosek, showing a generally low ozone values except for around October 1997, where the values peak to a maximum of about 55 DU. 1998 also follow the same trend, but with a much lower peak of about 35 DU also in October. These peak values are consistent with photochemical production of tropospheric ozone from biomass burning emissions in the Southern Asian region.

On the right hand side is that as derived for NH (Hohenpeissenbeg). Though, there are quite a lot of variations between sonde and FURM, a much generally higher values could be noticed as compared to the tropics (Watukosek). This could have been as a result of a significantly higher abundance of NO_x (the rate limiting ozone precursor) in the NH. The NH is more concentrated with higher industrial and transportation activities and so emissions from this region are expected to lead to significantly higher photochemical production of tropospheric ozone.

Another reason for the difference in trends in both locations could be due to the fact that there is a more efficient vertical transport in the tropics than the NH, making the tropical regions to be well mixed and allowing pollutants to be quickly washed away. Stratospheric influence is also quite lower in the tropics because of the much more stability in the tropopause height.

4.5 Inter-comparison between SONDE and two different versions of FURM

Shown here is an intercomparison between the sonde measurements for the two locations analysed and two different versions of the FURM algorithm.

The results derived from the version used in this study, which for simplicity purposes shall be to as version 1 is shown in red and that derived from a different version used by S.Tellmann referred (IUP, Bremen), also for the same reason shall be referred to as version 2 is shown in black (see figure 4.19).

This comparison is necessary so as to ascertain which of these versions is most suitable for tropospheric ozone vertical column retrieval in the tropical regions and the northern hemisphere. Listed in table 4.1 are the major differences between these two versions.

FURM by Amao [Version1]	**FURM by S. Tellmann [version 2]**
2 Channels; 290 – 302 (nm) and 320 – 355 (nm)	1 channel; 290 – 360 (nm)
Polynomial Subtraction	7 – 8 parameters to exclude calibration errors

Table 4.1 Main differences between two different versions of the FURM algorithm

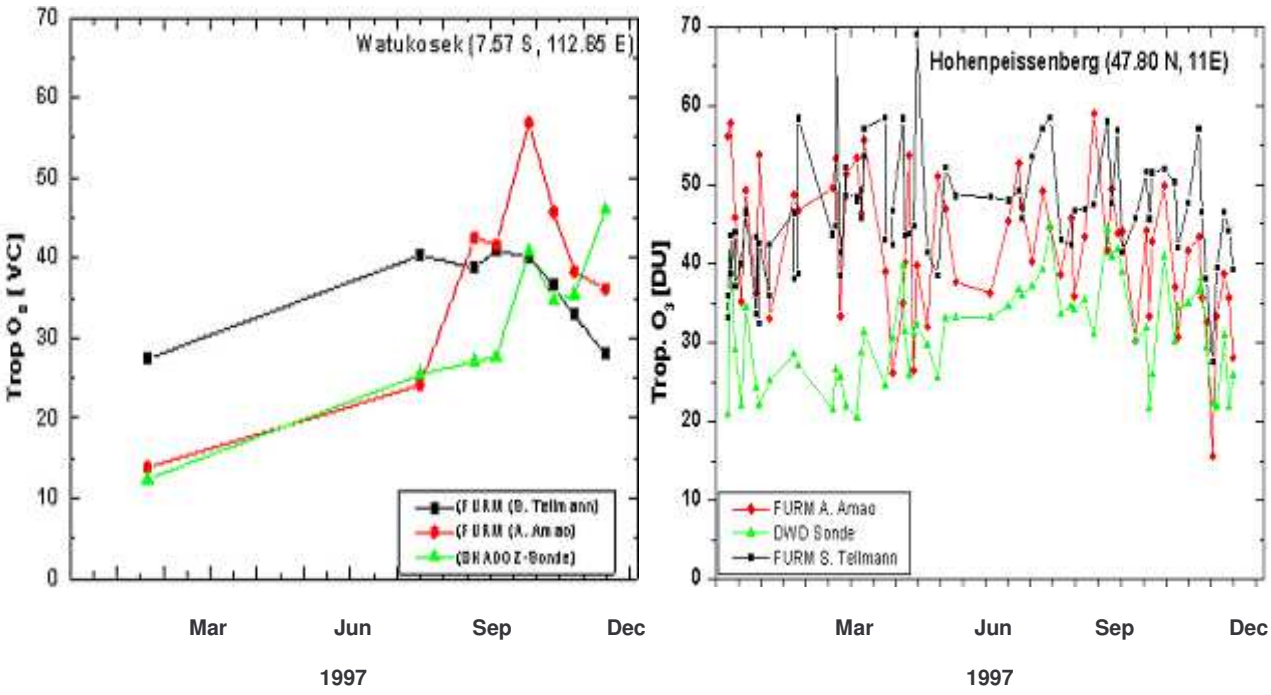

Figure 4.19 Tropospheric ozone vertical column from sonde as compared with two versions of FURM

Version 1 shows a much better agreement with sonde (green curve) as compared to version 2. The pattern shown in Hohenpeissenberg suggests that the two FURM versions are in agreement with each other, however the excess shown from January to March by version 1 seems to be more minimized as could be seen from the version 2 results.

In general, the version 1 gives a good retrieval capabilities in the tropics than than version 2. In the northern hemisphere however, results from both versions looks similar as compared to the sonde. Both results could have been affected by cloud presence or stratospheric intrusion.

4.6 Summary and Conclusion

Evidence of biomass burning could be seen from figure 4.4, where the ozone concentration peaks at around October to November 1997 and 1998. This period corresponds to the burning season at this region, where photochemical reactions involving NO_x and VOCs lead to photochemical production of tropospheric ozone.

El-Niño events are also seen to have influenced the photochemical production of tropospheric ozone in 1997 with a maximum ozone value of about 55 DU recorded. In 1998, the La-Niña conditions is a major factor in the much lower maximum of about 35 DU recorded during the biomass burning period.

The observation from sonde and the FURM result derived from GOME – data for Watukosek generally show good correlation (figure 4.6). The effect of Cloud coverage is not so pronounced in the derived result (see figure 4.7 and 4.8).

Results from Hohenpeissenberg, however shows very large variations between SONDE and FURM (see figures 4.11 and 4.12), especially in the in late winter towards early spring (Jan - April). The summer months however shows a much better agreement, probably as a result of a more stable tropopause height and also lesser cloud coverage at this period.

In 1998, the large variation in the early months still persists, extending to late spring. Stratospheric influence could have been responsible for these variations. And as was earlier seen better agreement was also observed in summer.

Cloud coverage also could have played a major role in the result derived from the northern hemisphere than in the tropics. Very cloudy scenario shows large differences.

The comparison between Hohenpeissenberg and Watukosek (section 4.4) gives an impression of higher photochemical production of tropospheric ozone in the northern hemisphere than in the tropics. Emissions of ozone precursors from industry and other urban related activities are more in abundance in the NH than in the tropics. The NH is also more influenced by tropopause folding, and as a result there exist more downward transport of lower stratospheric ozone into the upper troposphere. The maxima shown in the tropics between September and November 1997 and 1998 are also consistent with biomass burning emissions. From biomass burning activities precursors of ozone are emitted into the troposphere, which in the presence of sunlight is expected to lead to high tropospheric ozone production.

The version of the FUll Retrieval Method algorithm as used in deriving tropospheric ozone vertical column in this study shows a much better result in the tropic than in the northern hemisphere and also as compared to that used in deriving same by S. Tellmann.

Result from S. Tellmann also shows overestimated values in tropospheric ozone vertical column predominantly in the springs as was observed in figures 4.11 and 4.12.

Conclusively, the FURM shows good retrieval capabilities of tropospheric ozone vertical column in the tropics. Though with still some anomalies, this could be as a result measurement errors, error in calculating the radiances from a known ozone profile and in inverting the radiances to obtain an ozone profile.

The results from Hohenpeissenberg however suggest that the algorithms retrieval efficiency of tropospheric ozone vertical column is still not very effective in the NH.

As an outlook, the result from FURM algorithm in the NH could be improved upon probably by introducing in the algorithm a systematic way of determining the tropopause height instead of using the sonde ozone profile in defining it (which was the case in this study), before integrating to calculate the tropospheric ozone vertical column. Also determination of the tropopause height could be based upon the respective ozone profiles. That is, using sonde profile only in determining the tropopause height for sonde, while the profiles derived from GOME is used in determining that for FURM.

The FURM algorithm presently uses spectral information from Channel 1a (240-308 nm) and Channel 2 (316-400 nm). However, probably by including another channel such as channel 3 (400-605 nm) a much improved retrieval capabilities could be achieved.

References

Andrews, G. Davids, AnIntroduction to Atmospheric Physics, Cambridge University Press.

Brasseur, P. Guy, Orlando, J. John and Tyndall, S. Geoffery (1999). Atmospheric Chemistry and Global Change, Oxford University Press.

Brimblecombe, P. (1986). Air-Composition and Chemistry.

Burrows, J.P., Buchwitz, M., Rozanov, V., Weber, M., Richter, A., and Ladstätter-Weißenmayer, A. The Global Ozone Monitoring Experiment (GOME):Mission, Instrument Concept and First Scientific Results.

Colin, Baird (1995) Environmental Chemistry, Freeman and Company, New York.

Crutzen, P., Andrea, M. Biomass Burning in the Tropics – Impact on Atmospheric Chemistry and Biogeochemical Cycles.

Crutzen, P. Biomass Burning as a Source of Atmospheric Gases.

Eichmann, K-U., Bramstedt, K., Weber, M., Rozanov, V., deBeek, R., Hoogen, R., and Burrows, J.P. (2003). Ozone Profile Retrieval From GOME Satellite Data II: Validation and Applications.

Finlayson.Pitts, B., Pitts Jr, J.N. (1999). Chemistry of the Upper and Lower Atmosphere, Academic Press.

Jacob, D.J., (1999). Introduction to Atmospheric Chemistry, Princeton University Press.

John H. Seinfeld and Spyros N. Pandis ; Atmospheric Chemistry and Physics, John Wiley and sons,inc.

John T. Houghton. The Physics of Atmospheres, Cambridge University Press.

Kuo-Nan Liou ; An Introduction to Atmospheric Radiation, Academic Press, Inc.

Ladstätter-Weißenmayer, A., Burrows, J.P., Crutzen, P. and Richter, A. (1999). GOME: Biomass Burning and its Influence on the Troposphere, European Symposium on Atmospheric Measurements from Space.

Ladstätter-Weißenmayer, A. and Burrows, J.P. (1998). Biomass Burning Over Indonesia: Earth Observation Quarterly.

Levine, J.S., Bobbe, T., Ray, N., Witt, R.G., Singh, A. (1999). Wildland Fires and the Environment – A Global Synthesis.

Stephen, H. Stoker, Seager, S.I. (1976). Environmental Chemistry – Air and Water Pollution.

Wayne, R.P. (1991). Chemistry of the Atmospheres, Oxford University Press.

Wilgen, BW van, Andreae, MO., Goldammer, JG., Lindesay, JA., (1997). Fire in Southern African Savannas – Ecological and Atmospheric Prespective.

Acknowledgements

Firstly, I would like to show my gratitude to Prof. J.P. Burrows who gave me the opportunity to carry out this study under his supervision.

Special thanks and gratitude go to my tutor Dr. A. Ladstätter-Weißenmayer, who despite her very tight official schedule still find time to go through my work and offer useful and valuable advice.

I would like to thank Prof. J. Bleck-Neuhaus, Stefanie Raffalski and Barbara Kozak (the PEP team) for their support and assistance throughout my stay here.

I show my appreciation to Vladimir Rozanov who provided all details needed in the FURM algorithm and also S.Tellman for making her data available for comparison.

I must thank the entire DOAS group for their support and criticisms.

I cannot but show my most heart felt appreciation for the inspirational support from my parents, brothers and sisters.

My colleagues and other members of the IUP have also been of tremendous assistance.

Lastly and most importantly all glory is due to ALLAH for HIS mercies.